Cell Reports
Article

Cell PRESS
Open ACCESS

RNAi Factors Are Present and Active in Human Cell Nuclei

Keith T. Gagnon,[1,2] Liande Li,[1,2] Yongjun Chu,[1] Bethany A. Janowski,[1] and David R. Corey[1,*]
[1]Departments of Pharmacology and Biochemistry, University of Texas Southwestern Medical Center, Dallas, TX 75390-9041, USA
[2]These authors contributed equally to this work
*Correspondence: david.corey@utsouthwestern.edu
http://dx.doi.org/10.1016/j.celrep.2013.12.013

SUMMARY

RNAi is widely appreciated as a powerful regulator of mRNA translation in the cytoplasm of mammalian cells. However, the presence and activity of RNAi factors in the mammalian nucleus has been the subject of considerable debate. Here, we show that Argonaute-2 (Ago2) and RNAi factors Dicer, TRBP, and TRNC6A/GW182 are in the human nucleus and associate together in multiprotein complexes. Small RNAs can silence nuclear RNA and guide site-specific cleavage of the targeted RNA, demonstrating that RNAi can function in the human nucleus. Nuclear Dicer is active and miRNAs are bound to nuclear Ago2, consistent with the existence of nuclear miRNA pathways. Notably, we do not detect loading of duplex small RNAs in nuclear extracts and known loading factors are absent. These results extend RNAi into the mammalian nucleus and suggest that regulation of RNAi via small RNA loading of Ago2 differs between the cytoplasm and the nucleus.

INTRODUCTION

Since the discovery of mammalian RNAi (Elbashir et al., 2001), over 50,000 reports have described the use of small interfering RNAs (siRNAs). Almost all of these studies have assumed that the regulation of RNAi and its silencing activity occurs in the cytoplasm (Gurtan and Sharp, 2013). Whether RNAi can function in the mammalian nucleus and regulate processes like transcription or splicing has remained unclear (Castel and Martienssen, 2013; Harel-Bellan et al., 2013). Likewise, what role the nuclear compartment might play in the regulation of RNAi pathways is unknown. These uncertainties have significantly hampered investigation of nuclear RNA biology and the development of nuclear RNAi as a laboratory tool and potential therapeutic.

The assumption that mammalian RNAi is confined to the cytoplasm has been supported by reports that siRNAs cannot silence introns (Vickers et al., 2003; Zeng and Cullen, 2002). In addition, microscopy has shown a cytoplasmic distribution of RNAi factors, such as Argonaute-2 (Ago2), to P-bodies and the endoplasmic reticulum (ER) (Ikeda et al., 2006; Stalder et al., 2013). Some laboratories, however, have suggested that Ago2 and other RNAi factors can be found in the nucleus (Ando et al., 2011; Chu et al., 2010; Doyle et al., 2013; Ohrt et al., 2012; Rüdel et al., 2008; Till et al., 2007; Weinmann et al., 2009). siRNAs have been reported to silence the nuclear enriched RNAs 7SK and U6 (Ohrt et al., 2008; Robb et al., 2005). Although nuclear RNAi activity and localization of RNAi factors to the nucleus have been reported previously, questions about the purity of cell extracts (Holding, 2004), the resolution of localization studies, and nucleocytoplasmic transport of the RNA targets and products of RNAi have kept nuclear RNAi a controversial subject.

MicroRNAs (miRNAs) enter the RNAi pathway by binding Ago proteins (Gurtan and Sharp, 2013). In the cytoplasm, miRNAs guide Ago proteins to 3′ untranslated regions and destabilize or inhibit translation of mRNAs (Bartel, 2009; Gurtan and Sharp, 2013; Valencia-Sanchez et al., 2006). miRNAs have also been found in the nucleus (Jeffries et al., 2011; Katahira and Yoneda, 2011; Liao et al., 2010), but their biological roles are unknown. Both synthetic siRNAs and microRNAs have been shown to induce changes in splicing (Alló et al., 2009; Liu et al., 2012) and transcription (Janowski et al., 2007; Li et al., 2006; Matsui et al., 2013; Morris et al., 2004). However, the mechanisms mediating these processes remain controversial, due in part to the debate over the presence and activity of nuclear RNAi factors.

During cytoplasmic RNAi, small RNA loads into the RNA induced silencing complex (RISC), the complex recognizes a complementary RNA target, and target cleavage can occur at a specific site (Wilson and Doudna, 2013). Several factors have been implicated in the loading of small RNAs into Ago proteins (programming) and the maturation of RISC in human cells. These include the protein folding chaperones Hsp90 and Hsc70 (Iwasaki et al., 2010) and the component 3 promoter of RNAi (C3PO) complex composed of Translin and TRAX (Ye et al., 2011). Hsp90/Hsc70 are implicated in chaperone-like mechanisms that may open Ago proteins to accommodate the initial binding of a duplex RNA (Iwasaki et al., 2010). In addition, Hsp90 chaperone activity in RNAi programming and RISC maturation has been shown to be dependent on the presence of cochaperones, including Aha1, FKBP4/5, Cdc37, and p23 (Martinez et al., 2013; Pare et al., 2013). C3PO possesses single-strand nuclease activity and has been shown to accelerate passenger strand RNA removal from Ago to mature the RISC complex (Liu et al., 2009; Ye et al., 2011).

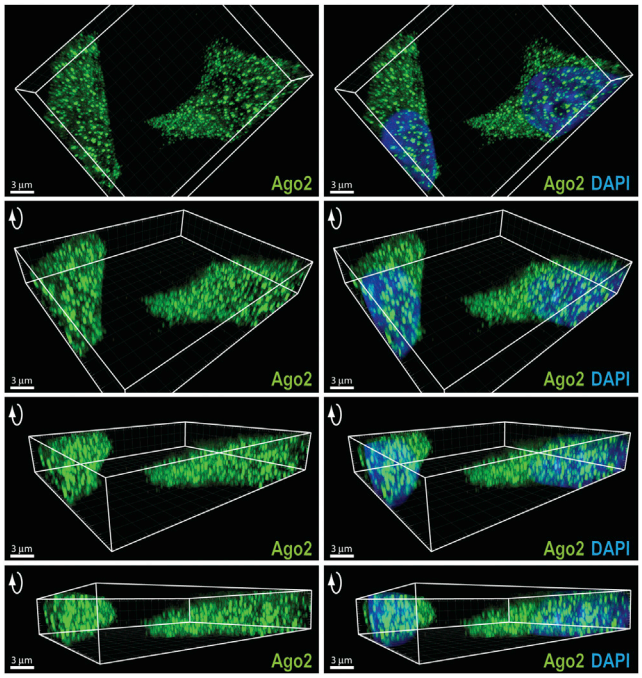

Figure 1. Microscopy Reveals Ago2 in Human Cell Nuclei
Immunofluorescence microscopy of endogenous Ago2 in HeLa cells. z sections are stacked (6 μm), projected three-dimensionally, and rotated to highlight nuclear staining. Scale bar represents 3 μm.

Ago2 binds small duplex RNA and forms the core of RISC (Hammond et al., 2000; MacRae et al., 2008; Wilson and Doudna, 2013). Other key players involved in RISC include the pre-miRNA processing enzyme Dicer, the TAR RNA-binding protein (TRBP), and TNRC6A (GW182 homolog) (Daniels and Gatignol, 2012; Lazzaretti et al., 2009; Ma et al., 2012; MacRae et al., 2008). Ago-RISC complexes recognize RNAs complementary to the guide strand (Hammond et al., 2000). When the guide strand is fully complementary to target RNA, Ago2 can catalyze site-specific phosphodiester bond cleavage ("slicer" activity) (Liu et al., 2004; Meister et al., 2004; Wang et al., 2008).

To resolve the controversy over mammalian nuclear RNAi, we investigated the localization, interaction, and activity of known RNAi factors in human cell nuclei. Here, we show that Ago2 and other RNAi factors are present in the nucleus and can associate in multiprotein complexes. Small RNAs in complex with Ago2 can silence nuclear RNA and induce site-specific cleavage. Nuclear Dicer is catalytically active and miRNAs are bound to nuclear Ago2. In contrast, we did not detect loading of duplex RNA in nuclei and most RISC loading factors are absent. These results place the protein machinery necessary for RNAi recognition inside the mammalian cell nucleus but suggest key differences between nuclear and cytoplasmic RNAi.

RESULTS

RNAi Factors Are Present in Human Cell Nuclei

We began our study by using HeLa cells to examine the localization of Ago2, the catalytic core of RNAi (Liu et al., 2004). We used wide-field immunoepifluorescence microscopy with blind deconvolution because the technique is ideal for rapid and high-sensitivity 3D imaging for thin specimens such as cells in monolayer culture (Shaw, 2006). In some cases, we also used confocal immunofluorescence microscopy for comparison. The success of immunofluorescence often depends on conditions like fixation and permeabilization, antibody binding, and cell type (Katikireddy and O'Sullivan, 2011). To improve detection of nuclear proteins, we used protocols designed to facilitate entry of antibody into the nucleus (Spector, 2011).

Our microscopy revealed a substantial amount of Ago2 in the nucleus in addition to the expected distribution within the cytoplasm. Images of slices through several micrometer thick sections along the z axis, combined with 3D rendering of composite focal sections, revealed Ago2 within the nuclear compartment (Figure 1; Movie S1). The application of two additional antibodies against human Ago2 produced similar results (Figures S1A–S1C), confirming that nuclear visualization was not due to off-target immunoreactivity. We also observed Ago2 in the nuclei of T47D breast cancer cells and fibroblast cells (Figures S1D–S1F), indicating that nuclear Ago2 is not cell type specific. Confocal microscopy confirmed nuclear localization of Ago2 (Figures S1G and S1H). We also used wide-field immunofluorescence microscopy to test localization of Dicer, TRBP, and TNRC6A and observed staining in the nucleus as well as in the cytoplasm (Figures S1I–S1K). These results using different microscopy platforms, cell lines, and detection reagents suggest the nuclear presence of the protein machinery that enables RNAi.

As a second method for testing nuclear localization, we used cellular fractionation and western blot analysis to evaluate the levels of Ago2 and other RNAi factors in the nucleus. We developed a stepwise protocol for isolating cytoplasmic, whole nuclear, nucleoplasmic (soluble nuclear), and chromatin-associated fractions from the same cell population. Fractions were used for various assays, including protein and RNA detection, chromatographic or biochemical fractionation, and enzymatic assays (Figure 2A).

RNAi factors can localize to the ER (Stalder et al., 2013). This poses a challenge for accurate assessment of localization inside of nuclei because the ER membrane is contiguous with the outer nuclear membrane (Hetzer, 2010). To ensure efficient removal of ER protein contamination, we tested detergents and conditions for preparation of nuclear extracts (Michelsen and von Hagen, 2009). Nuclei were washed with buffers containing different detergents and then visualized by fluorescence microscopy using DAPI and ER tracker, a fluorescent dye that binds the sulphonylurea receptor class of ER integral membrane proteins. Our microscopy indicated that the addition of 0.3% NP-40 was most efficient at removing ER contamination (Figure 2B). Western blots confirmed the absence of both ER lumen and ER membrane proteins from nuclear extracts (Figure 2C).

Western blot analysis of purified nuclei revealed endogenous Ago2, Dicer, TRBP, and TRNC6A in the nuclei of multiple human cell lines (Figure 2D). Protein markers for the cytoplasm, ER, and mitochondria were absent from nuclear preparations, consistent with stringent isolation of nuclei. Quantitation of western blots revealed relative nuclear abundances ranging from 40% to

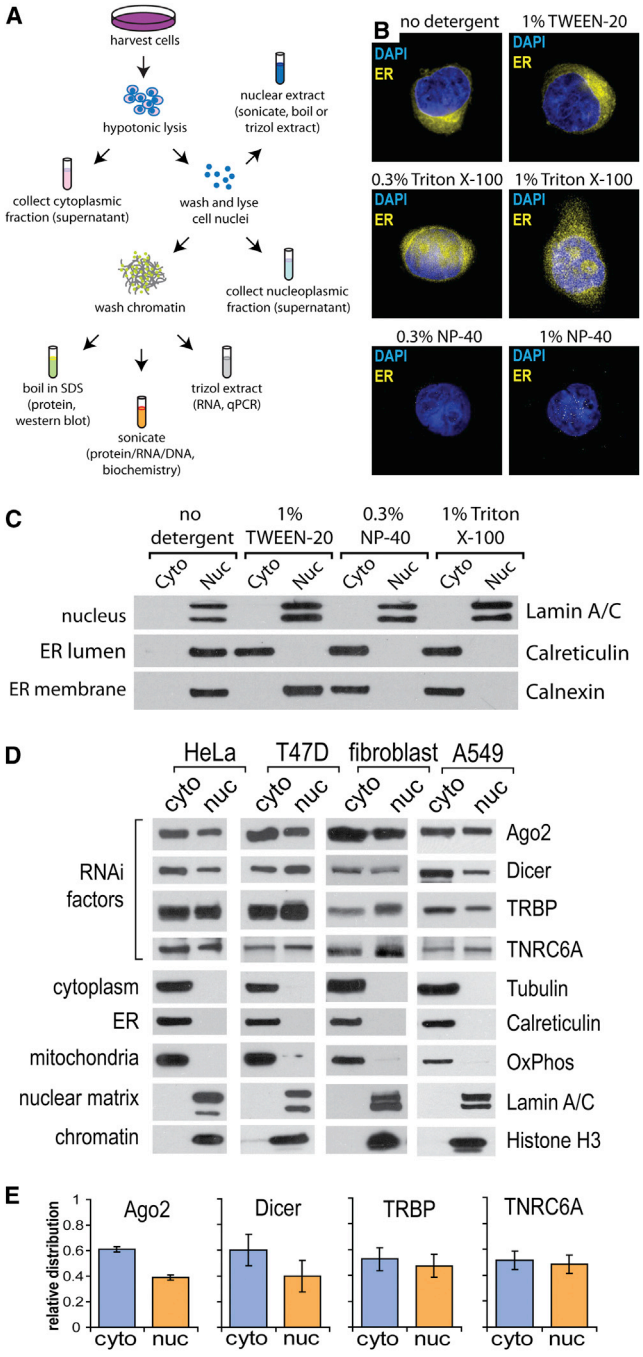

Figure 2. RNAi Factors Are Present in Nuclear Extracts

(A) Schematic of cellular fractionation protocol.

(B) Fluorescent imaging of intact HeLa nuclei after isolation with buffers containing different detergents. ER membrane is stained yellow with ER Tracker dye, DAPI staining of nuclei.

(C) Western blot analysis of cytoplasmic and nuclear fractions prepared with buffers containing different detergents. Calreticulin is a marker for the ER lumen. Calnexin is a marker for the ER membrane.

(D) Western blot of RNAi factors and subcellular markers from cytoplasmic and nuclear fractions prepared with 0.3% NP-40. Oxphos is a marker for mitochondria, Lamin A/C is a marker for nuclear matrix, and tubulin is a marker for cytoplam.

(E) Quantification of RNAi factors from western blots of HeLa, T47D, fibroblast, and A549 cells shown in (D). Error bar is ±SEM.

50% (Figure 2E). We also observed the other human Ago variants, Ago1, Ago3, and Ago4, in our nuclear preparations (Figure S2). Combined with microscopy, our analysis of cell fractions demonstrates that the basic machinery necessary to execute RNAi is present in human cell nuclei.

Nuclear RNAi Factors Can Stably Associate in Multiprotein Complexes

RNAi factors interact to form RISC and execute RNAi in the cytoplasm (MacRae et al., 2008; Wilson and Doudna, 2013). To determine whether nuclear RNAi factors also interact, we tested coimmunoprecipitations of nuclear Ago2, Dicer, TNRC6A, and TRBP. These coimmunoprecipitations revealed a network of interactions between RNAi factors (Figure 3A).

To further support the observed association of RNAi factors with Ago2 in nuclei, we generated T47D cells stably expressing FLAG-HA-tagged Ago2 (FHA-Ago2). Immunoprecipitation of FHA-Ago2 with FLAG antibody confirmed copurification of Dicer, TNRC6A, and TRBP (Figure 3B). Coimmunoprecipitation of Ago2 and Dicer or Ago2 and TNRC6A were also observed in nuclear extracts treated with RNase A, indicating that the association of RNAi factors was independent of RNA (Figure 3C).

To visualize the association of TNRC6A and Ago2 inside of cell nuclei, we performed immunofluorescence microscopy. These experiments revealed colocalization of Ago2 and TNRC6A staining within HeLa nuclei (Figures 3D and S3). Colocalization of Ago2 and TNRC6A is consistent with the suggestion from our coimmunoprecipitation results that nuclear RNAi factors can form complexes.

To further characterize nuclear complexes containing RNAi factors, we separated nuclear extracts by size and charge. Fractionation by size-exclusion chromatography revealed high molecular weight complexes containing all four RNAi factors (Figure 3E). To test the involvement of RNA in complex formation, we treated extracts with RNase A and observed that RNA was not required. When high molecular weight fractions containing RNAi factors were further separated by anion-exchange chromatography, RNAi factors continued to coelute (Figure 3F) indicating that the complexes were sufficiently stable to survive tandem purification schemes. Taken together, these results demonstrate that nuclear RNAi factors can form stable multiprotein RISC-like complexes.

To compare nuclear and cytoplasmic RNAi protein complexes, we performed similar size-exclusion chromatography with cytoplasmic extract (Figure 3G). The retention time of Ago2, Dicer, and TNRC6A was similar in cytoplasmic fractions compared to the nuclear fraction. TRBP, however, eluted later regardless of the presence or absence of RNase A. As an alternate test for the stability of complexes containing RNAi factors, we fractionated nuclear and cytoplasmic extracts by adding increasing amounts of ammonium sulfate. Although all four RNAi factors precipitated from nuclear extract at 20% ammonium sulfate, a 40% concentration was required for precipitation from cytoplasmic extract (Figure 3H). These results from

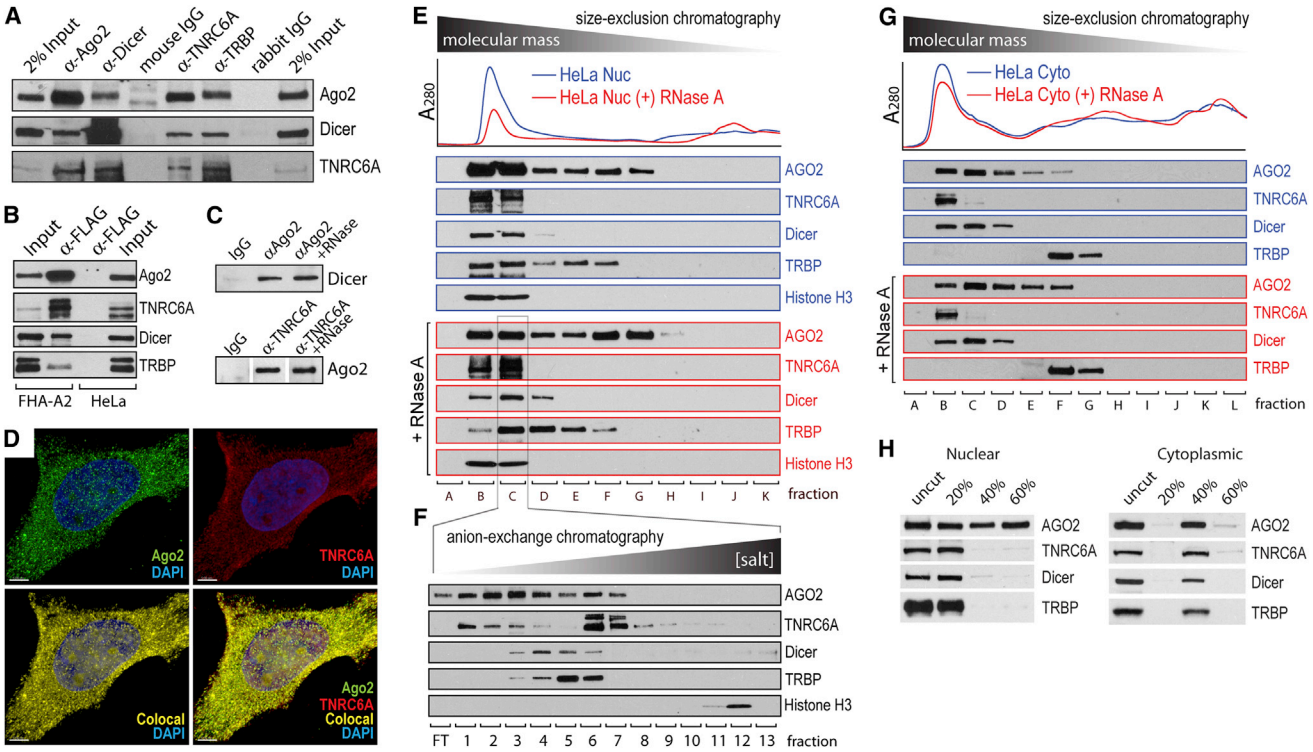

Figure 3. RNAi Factors Associate in Multiprotein Complexes in the Nucleus

(A) Coimmunoprecipitation (coIP) of endogenous RNAi factor from HeLa nuclear extract. The antibodies used for the western blot detection are noted to the right, whereas the antibodies used for immunoprecipitations are on top.

(B) CoIP of RNAi factors from T47D cells expressing FLAG-HA-tagged Ago2 (FHA-A2). HeLa nuclear extract serves as a negative control. Input is extract prior to immunoprecipitation.

(C) CoIP of Ago2 with Dicer or TNRC6A from T47D nuclear extracts treated with RNase A.

(D) Immunofluorescence of Ago2 and TNRC6A in HeLa cells indicates overlap and colocalization of immunostaining. z stacks (3 μm thickness taken in 0.1 μm slices) are projected in 3D. The colocalization channel was generated in Imaris (Bitplane). Scale bar represents 5 μm.

(E) Western analysis of fractions from separation of HeLa cell nuclear extract by size exclusion. Extracts were prepared either with our without treatment by RNase A. Western blot antibodies are shown to the right. Sample fractions are below. Histone H3 is marker for high molecular weight chromatin.

(F) Western analysis of fractions after anion-exchange chromatography of nuclear extract Fraction C from Figure 5E. FT, column flowthrough.

(G) Western analysis of fractions HeLa cytoplasmic extract after size-exclusion chromatography. Extracts were prepared either with our without treatment with RNase A.

(H) Effect of ammonium sulfate precipitation of RNAi factors from T47D nuclear or cytoplasmic extracts. Western blot antibodies are shown to the right and ammonium sulfate concentrations (% saturation) are shown above.

fractionation by either chromatography or precipitation reveal the formation of RISC-like complexes, but also suggest that the exact composition of complexes in the nucleus and the stability of their association differs from that observed in the cytoplasm.

RNAi Is Active in the Nucleus

After demonstrating that RNAi factors were present in human cell nuclei, we investigated whether they could also direct silencing of nuclear RNA substrates. We examined the silencing within cytoplasmic, nucleoplasmic, and chromatin-associated cell fractions. Our target RNAs were Malat1 and Neat1, long noncoding RNAs (lncRNAs) primarily associated with chromatin (Figure 4A) (Dodd et al., 2013). For comparison, we also targeted ribosomal protein L30 (RPL30) and peptidyl-prolyl isomerase A (PPIA) mRNAs, which are primarily cytoplasmic.

We treated cells with siRNAs targeting each RNA transcript, fractionated the cells, and then used quantitative PCR (qPCR) to measure RNA levels. As typically observed with siRNAs, levels of all four RNA transcripts were reduced in the cytoplasmic fraction (Figure 4B). We observed a similar reduction of transcript levels in nucleoplasmic and chromatin fractions, consistent with RNAi activity in nuclei (Figure 4B).

Cleavage at a predicted location is a diagnostic for substrate processing by Ago2. Therefore, we used 5′ rapid amplification of cDNA ends (5′ RACE) to further test whether silencing of RNA in the nucleoplasm and on chromatin was due to Ago2-mediated cleavage. We isolated RACE products and sequencing revealed that site-specific cleavage had occurred at the predicted phosphodiester bond in all cellular fractions for Malat1 (Figures 4C, S4A, and S4B). Identification of the predicted RACE products associated with chromatin and in nucleoplasm is additional evidence for nuclear RNAi activity.

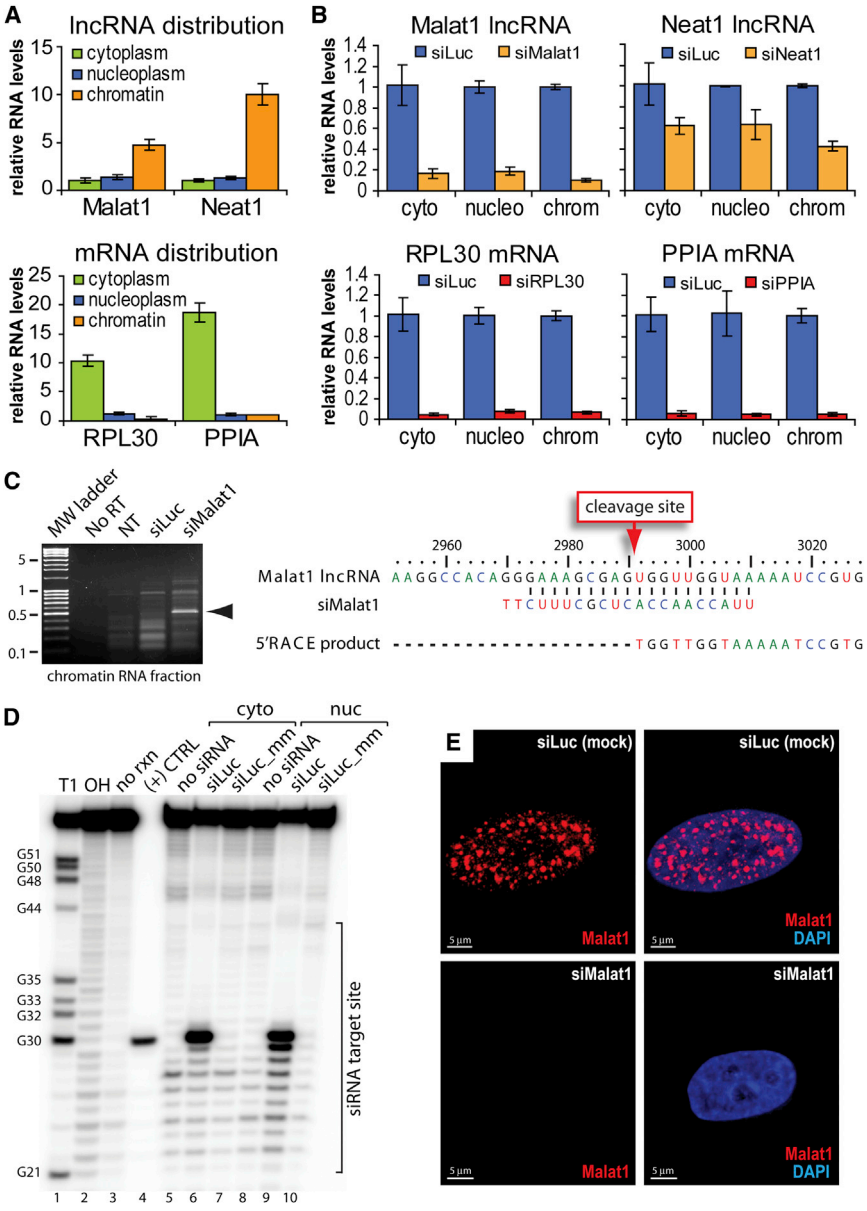

Figure 4. RNAi Is Active in the Human Cell Nucleus

(A) Quantification RNA distribution in HeLa subcellular fractions by qPCR. Error bar is ±SEM.

(B) Quantification by qPCR of siRNA-mediated lncRNA and mRNA knockdown in HeLa subcellular fractions. Error bar is ±SEM

(C) 5′ RACE to detect siRNA-mediated Ago2 cleavage of Malat1 in chromatin-associated RNA fractions. Arrow indicates specific cleavage product.

(D) Cleavage of a 5′-radiolabeled luciferase RNA substrate by Ago2 isolated from cytoplasmic or nuclear fractions. T1, RNase T1 cleavage; OH, alkaline hydrolysis; (+) CTRL, synthetic cleavage product. The region overlapped by the siRNA is noted.

(E) FISH showing that Malat1 speckles in HeLa cells are lost upon treatment with siMalat1 siRNA. z stacks are 5 μm thickness. siLuc, mock treatment. Scale bar represents 5 μm.

To further investigate the potential for nuclear Ago2 to cleave RNA substrates, we set up an in vitro cleavage assay using Ago2 from either cytoplasmic or nuclear fractions and a radiolabeled RNA substrate derived from luciferase (Luc) mRNA (Elbashir et al., 2001). Cells were transfected with a duplex RNA (siLuc) complementary to the Luc RNA substrate or a duplex RNA containing two central mismatches (siLuc_mm). Central mismatches are known to disrupt slicer activity (Wang et al., 2008). Ago2 was then immunoprecipitated from either the cytoplasmic or nuclear fractions and incubated with the radiolabeled target RNA substrate. Reactions were then resolved on denaturing polyacrylamide gels to visualize cleavage products.

Ago2 immunoprecipitated from both cytoplasmic and nuclear extracts of cells treated with siLuc caused sequence-specific cleavage of the Luc substrate (Figure 4D, lanes 6 and 9). In contrast, Ago2 from cytoplasmic and nuclear extracts of cells treated with siLuc_mm did not support cleavage (Figure 4D, lanes 7 and 10). A lack of cleavage for siLuc_mm is expected based on the known slicer mechanism of Ago2, which requires perfect complementarity at the targeted bond (Wang et al., 2008). These results demonstrate sequence-specific slicer activity for nuclear Ago2.

To visualize RNAi-mediated activity inside cell nuclei, we targeted Malat1 RNA with a siRNA (siMalat1) and performed fluorescence in situ hybridization (FISH). FISH prior to siMalat1 treatment revealed distinct nuclear speckles. Upon treatment with siMalat1, the Malat1 speckles disappeared. In contrast to the disappearance of speckles after treatment with siMalat1, a siRNA with no cellular target (siLuc) had no effect (Figures 4E, S4C, and S4D). Taken together, several lines of evidence are consistent with RNAi slicer activity in cell nuclei, including (1) siRNA-mediated reduction in the levels of nuclear RNA targets, (2) site-specific cleavage of nuclear RNA targets at a position diagnostic for RNAi, (3) cleavage of target RNA by Ago 2 isolated from nuclear extract, and (4) visualization of reduced target RNA within cell nuclei.

miRNAs in Cell Nuclei

We evaluated the localization of miRNAs within cell nuclei and their association with Ago2. Sequencing of small RNAs revealed that out of 456 miRNA species identified in the whole cell, 346 of them also exist in cell nuclei, suggesting that roughly 75% of miRNAs in the cytoplasm are shuttled into the cell nucleus

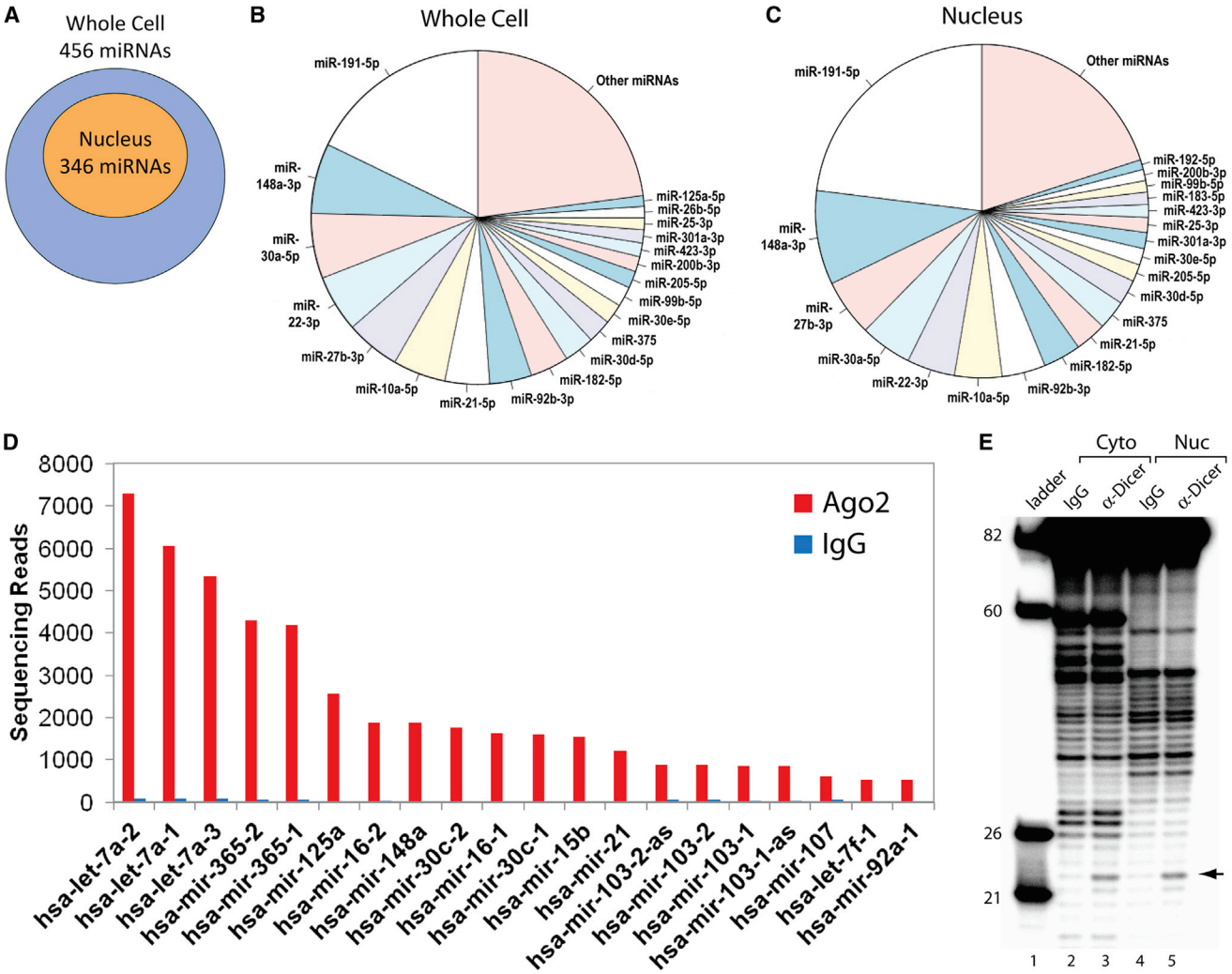

Figure 5. miRNAs Are in the Nucleus and Associate with Ago2

(A) Distribution of miRNAs by single molecule small RNA sequencing in nuclei versus whole cell.

(B and C) Relative abundance of top 20 miRNAs in whole-cell versus nuclear fractions.

(D) Top 20 miRNAs bound to nuclear Ago2 identified by immunoprecipitation and single molecule small RNA sequencing. Results are compared to a negative control from immunoprecipitation using a nonspecific antibody (IgG).

(E) Detection of processing products from cytoplasmic and nuclear Dicer. RNA molecular weight ladder is shown to the left (lane 1). Arrow indicates specific Dicer processing product band.

(Figure 5A). The identities of many of the top 18 ranked miRNAs, based on the number of obtained sequencing reads, were the same between nuclei and whole cell (Figures 5B and 5C), indicating a similar distribution of abundant miRNA species in the cytoplasm and the nucleus.

We then examined the association of miRNAs with Ago2 in cell nuclei. Ago2 was immunoprecipitated from nuclear extract using a nonspecific mouse immunoglobulin G (IgG) as a negative control. Bound small RNAs were isolated and sequenced on a Helicos single molecule sequencer using direct RNA sequencing mode. In this mode, the steps of making complementary DNA and PCR amplification are avoided so that potential sequencing biases are eliminated. The number of sequencing reads better represents the original miRNA expression level. We prepared two biological replicates and averaged the sequencing read number for each small RNA. Single molecule sequencing revealed substantial binding of numerous miRNAs to nuclear Ago2 (Figure 5D).

To further examine the potential for miRNA pathways to operate in the nucleus, we tested the ability of Dicer, the enzyme that processes pre-miRNA precursors, to generate mature miRNAs in nuclear or cytoplasmic extracts. We performed an in vitro processing assay in which we immunoprecipitated Dicer from cytoplasmic or nuclear extracts, mixed it with radiolabeled pre-miR-19a, and analyzed cleavage products by denaturing polyacrylamide gel electrophoresis. We observed the expected 23 nucleotide product for both nuclear- and cytoplasmic-derived Dicer (Figure 5E). These results suggest that Dicer can process

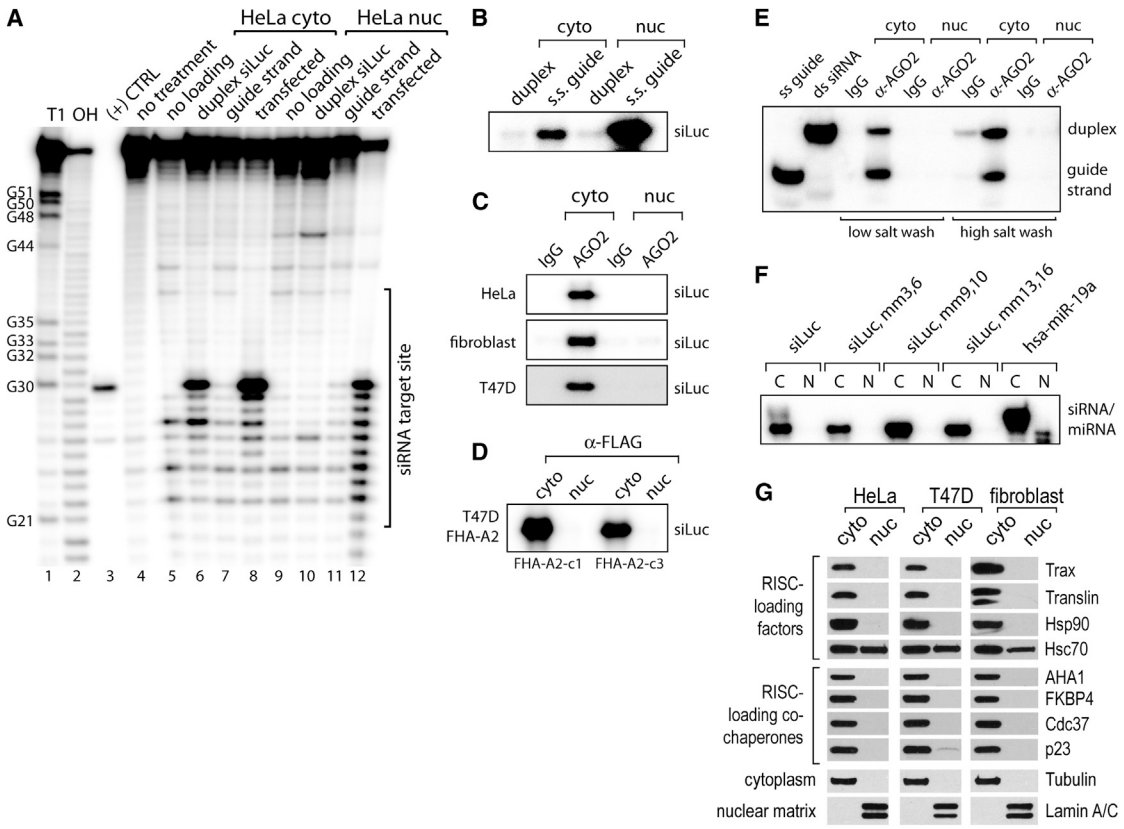

Figure 6. Duplex Small RNA Loading Is Deficient and RISC Loading Factors Are Absent in Nuclear Extracts

(A) Cleavage of a 5′-radiolabeled luciferase RNA substrate by Ago2 isolated from cytoplasmic or nuclear fractions treated as shown above the gel. T1, RNase T1 cleavage; OH, alkaline hydrolysis; (+) CTRL, synthetic cleavage product.

(B) Coprecipitation of radiolabeled duplex siLuc or radiolabeled single-strand siLuc guide RNA incubated with Ago2 after immunoprecipitation from nuclear or cytoplasmic extracts.

(C and D) In vitro assay for Ago2 duplex siRNA loading in extracts. Radiolabeled siRNA is added to extracts from human cell lines, Ago2 immunoprecipitated with Ago2 or FLAG antibody, and copurified RNA resolved on a denaturing polyacrylamide gel. FHA-A2-c1 and FHA-A2-c3 are two different T47D clonal cell lines stably expressing FLAG-HA-tagged Ago2.

(E) Radiolabeled siLuc was used in the same assay shown in (C) and (D), but copurified RNA was resolved on a nondenaturing polyacrylamide gel. Immunoprecipitation wash conditions and shown below the gel and the copurified duplex or single-strand RNAs indicated to the right.

(F) Radiolabeled miR-19a or siLuc were used in the same assay shown in (C) and (D). Mismatch positions relative to the 5′ end of the guide strand are indicated above the gel.

(G) Western blot of RISC loading and maturation factors and subcellular markers from cytoplasmic and nuclear fractions.

pre-miRNAs in the nucleus and is consistent with the potential for nuclear regulation and production of small RNAs.

Small Duplex RNA Loading of Ago2 Is Deficient in Nuclear Extract

Observed differences in fractionation of nuclear versus cytoplasmic RNAi factor complexes (Figure 3) suggested that other differences between cytoplasmic and nuclear RISC might exist. To extend our analysis, we tested whether there might be differences in small RNA loading between the nucleus and cytoplasm.

When examining Ago2 slicer activity in vitro (Figure 4D), our extracts were initially prepared from cells that were transfected with siRNA. This protocol requires the RNA to pass through the cytoplasm before entering the nucleus, and therefore loading might occur in the cytoplasm. Subsequent nuclear import of loaded Ago2 complexes might then account for the slicer activity observed in the nucleus (Ohrt et al., 2008; Weinmann et al., 2009). To determine where loading was occurring, we added small RNAs directly to nuclear extracts prepared from untreated cells and subsequently performed in vitro assays for slicer activity.

As we had observed previously, when Ago2 is isolated from extracts of cells transfected with siLuc, Ago2 from both the cytoplasm and nucleus can catalyze cleavage of the Luc substrate RNA (Figure 6A, lanes 8 and 12). By contrast, extracts from untransfected cells where double-stranded siLuc was added after extract preparation revealed that cytoplasmic Ago2 was able to catalyze cleavage but that nuclear Ago2 was inactive (Figure 6A, lanes 6 and 10). These data are consistent with nuclear slicer activity and replicate our previous findings (Figure 4), but also suggest a deficiency in Ago2 loading in nuclear extracts.

We further examined the loading of single-stranded guide RNA alone. Single-stranded RNAs are usually rapidly degraded

in cell extracts, precluding efficient loading. Nevertheless we found that addition of the single-stranded siLuc guide strand conferred low but similar levels of cleavage for both cytoplasmic and nuclear Ago2 (Figure 6A, lanes 7 and 11).

RNA single strands can be directly bound by Ago2 without the need for additional factors (Rivas et al., 2005). As a control to ensure that nuclear Ago2 was accessible for loading, we immunoprecipitated Ago2 and then incubated it with a radiolabeled single-strand siLuc guide RNA. We found that both cytoplasmic and nuclear Ago2 were able to bind the single-stranded guide (Figures 6B and S5A). Taken together, our observations that Ago2 from nuclear extract can (1) direct cleavage of an RNA target after mixing with single-stranded but not duplex RNA and (2) bind single-strand RNA are consistent with the loading of duplex RNA being deficient in cell nuclei.

Because duplex RNAs are susceptible to degradation by nucleases (Braasch et al., 2003), we considered the possibility that nuclear extracts could harbor a nuclease activity that might interfere with loading. When duplex RNA was incubated with either nuclear or cytoplasmic extracts, we observed similar levels of degradation over time (Figure S5B), suggesting that nuclease activity cannot explain our findings.

To more directly investigate Ago2 loading with duplex small RNA, we developed an in vitro loading assay. We added duplex siLuc with a radiolabeled guide strand to either nuclear or cytoplasmic extracts. When Ago2 was immunoprecipitated with antibodies against either endogenous or FLAG-tagged Ago2, we observed copurification of radiolabeled siLuc guide strand with cytoplasmic, but not nuclear, Ago2 (Figures 6C and 6D). A lack of nuclear loading was still observed when both siLuc strands were radiolabeled, ruling out a potential passenger strand loading bias in the nucleus (Figure S5C). We also confirmed that similar amounts of Ago2 were immunoprecipitated from both extracts in our experiments (Figure S5D). Nuclear extracts are unlikely to support efficient ATP regeneration for some RNAi processes (Klouwen and Appelman, 1967; Zamore et al., 2000). Because RISC loading has been reported to require ATP (Iwasaki et al., 2010), we used phosphocreatine and creatine kinase (Calhoun and Swartz, 2007) to regenerate ATP. We observed no change in loading in the nuclear extract (Figure S5E), excluding insufficient ATP as a possible explanation for the duplex loading deficiency.

Small duplex RNA loading involves an initial step when the duplex first binds to RISC and an unwinding step when the passenger strand is removed (Iwasaki et al., 2010; Matranga et al., 2005; Ye et al., 2011). To determine the limiting step in nuclear loading, we performed the in vitro Ago2 loading assay under conditions that would discriminate between duplex siRNA or single-strand guide RNA bound to Ago2. Immunoprecipitations were washed with the standard high-salt (0.5 M NaCl) buffer or with a low-salt (0.15 M NaCl) buffer to potentially preserve formation of unstable Ago2-RNA complexes. When RNA isolated from Ago2 immunoprecipitations was resolved by native gel electrophoresis, both duplex and single-stranded RNAs were bound to cytoplasmic Ago2, indicating formation of both complexes during loading (Figure 6E). In contrast, neither complex was formed during loading in nuclear extracts. This result demonstrates that the initial step of duplex RNA loading is deficient in nuclear extracts.

Our observation of miRNAs and Dicer activity in cell nuclei (Figure 5) led us to examine loading of miRNAs. We tested loading of a miR-19a duplex miRNA and duplex RNAs based on siLuc that contained central or terminal mismatches. Like fully complementary RNAs, we observed that mismatched duplexes were loaded in cytoplasmic extract but were not loaded in nuclear extract (Figure 6F). These results suggest that duplex miRNAs may also be differentially loaded between the nucleus and the cytoplasm.

Because several proteins are implicated in Ago2 loading and RISC maturation (Iwasaki et al., 2010; Pare et al., 2013; Ye et al., 2011), we performed western blot to detect their presence in isolated nuclei. Surprisingly, these loading factors, Hsp90, Translin, TRAX, Aha1, FKBP4, Cdc37 and p23, were all exclusively cytoplasmic (Figure 6G). The only exception was Hsc70, which was found in both the nucleus and the cytoplasm. These results are consistent with a loading restriction to the cytoplasm and suggest that programming of RNAi via Ago loading is regulated by exclusion of critical loading factors from the nucleus.

DISCUSSION

There has been conflicting evidence over the presence and activity of canonical RNAi factors in mammalian somatic cell nuclei. The biological significance of the nucleus in the regulation of RNAi pathways has also been unclear. This uncertainty has obscured the potential for small RNAs to participate in the regulation of nuclear processes. In this study, we used multiple methods to test whether RNAi factors and RNAi activity could be detected in mammalian cell nuclei. We employed protocols for purifying nuclei that are free of ER protein contamination for in vitro analyses and methods for visualizing RNAi factors and RNAi activity in cell nuclei.

Our complementary experimental approaches support the existence of nuclear RNAi but also indicate that it differs from cytoplasmic RNAi. We find that (1) Ago2, the catalytic engine of RNAi, and the RNAi factors Dicer, TRBP, and TNRC6A are all present in human cell nuclei; (2) these nuclear-localized RNAi factors can associate in stable multiprotein complexes; (3) small RNAs can reduce levels of nuclear-localized RNA targets through site-specific cleavage; (4) Ago2 and Dicer isolated from nuclei exhibit catalytic activity; (5) the effects of RNAi activity can be visualized inside of human cell nuclei by FISH; (6) endogenous miRNAs are bound to nuclear Ago2 and miRNA pathway components are in the nucleus; (7) programming of RNAi through Ago2 loading with duplex small RNAs is not observed in nuclear extracts; and (8) necessary RISC loading and maturation factors are absent from the nucleus.

A previous study from Meister and colleagues reported on the presence and complex formation of EGFP-tagged Ago2 in human cell nuclei using fluorescence correlation and cross-correlation spectroscopy (Ohrt et al., 2008). Consistent with their results, we also observed Ago2 in the nucleus. However, they found that nuclear EGFP-Ago2 did not appear to associate with large complexes. These differences may be accounted for by our focus on endogenous Ago2 and by variations in

fractionation techniques. Based on spectroscopy data, Ohrt et al. (2008) also proposed that Ago2 is loaded in the cytoplasm and imported into the nucleus. Our data support this hypothesis with biochemical evidence and provide a potential explanation by observing a nuclear absence of the known RISC loading factors. The exclusion of RNAi programming from the nucleus has important implications for RNAi because small RNAs that are primarily nuclear may be loaded inefficiently or not at all. This partitioning of RISC loading may have evolved to regulate the involvement of nuclear small RNA in RNAi-mediated processes.

The activity and regulation of RNAi factors in mammalian cell nuclei might have multiple impacts on gene regulation. Small RNAs could potentially guide RNAi factors like Argonaute to nuclear RNA species, such as noncoding RNAs at gene promoters to affect transcription or intronic RNA to alter splicing. Nuclear RNAi-like pathways exist in various eukaryotic organisms like plants, flies, worms, fungi, and ciliated protozoa (Castel and Martienssen, 2013; Gagnon and Corey, 2012). These pathways have been characterized to regulate processes like nuclear gene expression, epigenetic states, and genome maintenance (Malone and Hannon, 2009). The demonstrated presence and activity of canonical RNAi factors in mammalian cell nuclei suggest that similar pathways may exist in humans.

We have recently reported a role for Ago2 and TNRC6A in endogenous control of the inflammatory pathway genes cyclooxygenase 2 (COX-2) and phospholipase 2G 4A (PLA2G4A) by miR-589 miRNA (Matsui et al., 2013). COX-2 and PLA2G4A are adjacent genes whose promoters are linked by chromosomal looping. miR-589 is expressed in A549 lung cancer cells and has two seed sequence target sites at the COX-2 promoter. Elevated levels of miR-589 lead to increased expression of both COX-2 and PLA2G4A. Ago2 and TNRC6A are recruited by miR-589 to a sense transcript that overlaps the COX-2 promoter. When Ago2 or TNRC6A levels are depleted, the activation of COX-2 and PLA2G4A by miR-589 is reversed. These results provide an experimental demonstration that nuclear RNAi factors can play a role in regulating a physiologically important regulatory pathway.

Mammalian RNAi has typically been assumed to localize to the cytoplasm, limiting the vision of researchers investigating the regulation of gene expression. Clarity about RNAi factors and their activity in the nucleus widens investigation of RNAi beyond traditional targets in the cytoplasm to targets in the nucleus that may regulate processes like transcription or splicing. Although much remains to be learned about nuclear RNAi, such control in the nucleus would add a new layer of gene regulation and offer new options for RNAi-based therapeutics.

EXPERIMENTAL PROCEDURES

Tissue Culture and siRNA Transfection

HeLa, T47D, fibroblast, and A549 cells were cultured in their standard media at 37°C in 5% CO_2. Lipofectamine RNAiMAX (Invitrogen) was used to deliver siRNAs into cells following the manufacturer's recommended protocol. Sequences of siRNAs used are listed in Table S1.

Nuclear and Cytoplasmic Cell Fractions

Cells were lysed in hypotonic lysis buffer (HLB) (10 mM Tris-HCl [pH 7.5], 10 mM NaCl, 3 mM $MgCl_2$, 0.3% NP-40) supplemented with 1% Protease Inhibitor (PI), 1 mM NaF, and 1 mM Na_3VO_4. Cells were spun and supernatant kept as cytoplasmic extract after addition of NaCl to 0.15 M and glycerol to 10%. Pelleted nuclei were washed three times with HLB. To make nuclear extract, nuclei were resuspended in nuclear lysis buffer (same as HLB but containing 0.15 M NaCl and 10% glycerol) also supplemented with PI, NaF, and Na_3VO_4. Nuclei were sonicated and supernatant kept as nuclear extract.

Coimmunoprecipitation

Protein G Plus/Protein A resin (Calbiochem), antibody and precleared nuclear extract were mixed at 4°C for 2–3 hr. When indicated, 20 μg RNase A was added before incubation. Resin was washed with IP wash buffer (20 mM Tris-HCl [pH 7.5], 0.4 M NaCl, 2 mM $MgCl_2$, 0.05% NP-40, 0.025% SDS) and copurified proteins eluted with SDS-PAGE loading buffer. Specific proteins were detected by western blot.

Chromatographic Separation and Ammonium Sulfate Cuts of Cell Extracts

For size-exclusion chromatography, extracts were either treated with RNase A or SUPERase-In (Ambion), filtered, injected onto a Superdex 200 HiLoad 16/60 column (Amersham Pharmacia) preequilibrated with FPLC buffer (20 mM Tris-HCl [pH 7.5], 150 mM NaCl, 3 mM $MgCl_2$, 5% glycerol), and separated by FPLC. Eluted fractions were assayed by western blot. For subsequent fractionation by anion exchange, size-exclusion fractions were concentrated and injected onto a Mono-Q FPLC column (Amersham Pharmacia) equilibrated with FPLC buffer at 0.1 M NaCl. Elution was performed by linear gradient from 0.1 to 1 M NaCl. For ammonium sulfate precipitation, saturated ammonium sulfate solution was added to cell extracts at the indicated final percentages, incubated on ice for 15 min, spun down at 18,000 × *g* at room temperature, and pelleted precipitate resuspended in SDS loading buffer. Supernatant was kept and additional ammonium sulfate added for the next cut. Fractions were analyzed by western blot.

Analysis of siRNA-Mediated RNA Knockdown in Cellular Compartments

HeLa cells were transfected with 25 nM siRNA and then harvested 72 hr later. Cells were counted and fractionated similarly to above. However, instead of sonicating, nuclei were lysed with modified Wuarin-Schibler buffer (MWS) (10 mM Tris-HCl [pH 7.0], 4 mM EDTA, 0.3 M NaCl, 1 M urea, 1% NP-40) (Wuarin and Schibler, 1994). Supernatant was kept as nucleoplasmic fraction and chromatin washed. RNA was isolated from cytoplasmic and nucleoplasmic fractions by precipitation and Trizol extraction. RNA was isolated from chromatin by Trizol extraction.

In Vitro Ago2 Cleavage Assay

HeLa cells were either untreated or transfected with 25 nM siLuc or siLuc_mm (see Table S1) and then harvested 36 hr later, and nuclear and cytoplasmic extracts were prepared. When indicated, siRNA or single-strand guide RNA was incubated with extract from untreated cells for 1 hr at room temperature with rotation. Ago2 was immunoprecipitated using Ago2 antibody (Abcam, ab57113), Protein G Plus/Protein A agarose (Calbiochem), and 200 μl extract at room temperature rotation for 1 hr. Resin was washed with IP wash buffer (IPWB) (20 mM Tris-HCl [pH 7.5], 4 mM $MgCl_2$, 0.5 M NaCl, 0.05% NP-40) and then mixed with 5′ radiolabeled synthetic target RNA substrate in 1 × RNAi buffer (20 mM Tris-HCl [pH 7.5], 4 mM $MgCl_2$, 0.5 mM DTT, 80 mM NaCl, 20 mM KCl, 0.5 mM EDTA) supplemented with 1 mg/ml yeast tRNA, 20 units SUPERase-In (Ambion), and 0.5 mM ATP. Reactions were incubated at 30°C for 1.5 hr with periodic mixing, and then target RNA and cleavage products were phenol extracted. Extracted RNA was resolved on a 15% denaturing polyacrylamide sequencing gel. The gel was dried and exposed to a phosphorimager screen overnight to visualize radioactive bands.

Immunofluorescence and Colocalization Analysis

Immunofluorescence was performed similarly to that previously described (Ohrt et al., 2012; Spector, 2011) with modifications. Briefly, cells were grown on 35 mm dishes with a 14 mm glass bottom. Cells were fixed in 2% formaldehyde or 4% paraformaldehyde. Fixed cells were then permeabilized with 0.2% Triton X-100 or 70% ethanol. Cells were incubated in primary antibody

in PBS + 1% normal goat serum (NGS), washed, incubated with secondary antibody + 1% NGS, washed again, and then set in mounting medium with DAPI and imaged. Cells were imaged by wide-field epifluorescence microscopy and images processed by blind deconvolution with AutoQuant X3 (Media Cybernetics). Alternatively, some samples were imaged by Andor spin disc confocal microscopy. Colocalization channels were calculated using Imaris (Bitplane) based on the correlation of the strength of linear relation between the two channels. Threshold levels for calculation were selected above background.

Fluorescence in Situ Hybridization

Cells were grown on 35 mm MatTek dishes and transfected with 25 nM siLuc or siMalat1 as described above. Cells were fixed in ice-cold 4% PFA and permeabilized in 70%. From this point forward, the protocol recommended by the manufacturer of the FISH probes for Malat-1 (Biosearch Technologies, New Stellaris RNA FISH Probe for Malat-1, SMF-2035-1) was followed. Cells were set with mounting medium with DAPI and imaged as above for IF.

Small RNA Sequencing

Small RNA sequencing libraries were constructed from either whole-cell RNAs or nuclear RNAs isolated from T47D cells and sequenced on Illumina Hiseq 2000. The reads were aligned to human genome hg19, UCSC miRNA database, and/or miRBase (mature miRNA).

Ago2-associated miRNA in cell nucleus was isolated by RNA immunoprecipitation using a specific Ago2 antibody. Small RNA (<40 nt) including miRNA was further isolated by gel purification. The small RNA was then subjected to poly(A) tailing and sequenced on a single-molecule Helicos sequencer with a Direct RNA Sequencing (DRS) module.

In Vitro Ago2 Small RNA Loading Assay

Duplex siRNA or single-strand guide RNA radiolabeled at the 5′ end was incubated with extract supplemented with 1 mM ATP for 1 hr at room temperature with rotation. Ago2 was immunoprecipitated using Ago2 antibody (Abcam, ab57113) and Protein G Plus/Protein A agarose (Calbiochem). Resin was washed with IP wash buffer (IPWB) (20 mM Tris-HCl [pH 7.5], 4 mM $MgCl_2$, 0.5 M NaCl, 0.05% NP-40) and then phenol-chloroform extract to isolate copurified RNA. Extracted RNA was resolved on a 15% denaturing polyacrylamide sequencing gel or a 15% native TBE-buffered polyacrylamide gel. The gel was dried and exposed to a phosphorimager screen overnight to visualize radioactive bands.

SUPPLEMENTAL INFORMATION

Supplemental Information includes Supplemental Experimental Procedures, five figures, one table, and one movie and can be found with this article online at http://dx.doi.org/10.1016/j.celrep.2013.12.013.

ACKNOWLEDGMENTS

This work was supported by the National Institutes of Health (1F32HD060377, to K.T.G.; GM 73042, to D.R.C., and GM85080, to B.A.J.), the Welch Foundation (I-1244, to D.R.C.), and the Cancer Prevention and Research Institute of Texas (RP120311, to B.A.J.). We thank R. Kalantari for sharing cell lines stably expressing FLAG-HA-tagged Ago2, Q. Liu for reagents, and J.K. Watts for comments.

Received: September 3, 2013
Revised: November 12, 2013
Accepted: December 6, 2013
Published: January 2, 2014

REFERENCES

Alló, M., Buggiano, V., Fededa, J.P., Petrillo, E., Schor, I., de la Mata, M., Agirre, E., Plass, M., Eyras, E., Elela, S.A., et al. (2009). Control of alternative splicing through siRNA-mediated transcriptional gene silencing. Nat. Struct. Mol. Biol. *16*, 717–724.

Ando, Y., Tomaru, Y., Morinaga, A., Burroughs, A.M., Kawaji, H., Kubosaki, A., Kimura, R., Tagata, M., Ino, Y., Hirano, H., et al. (2011). Nuclear pore complex protein mediated nuclear localization of dicer protein in human cells. PLoS ONE *6*, e23385.

Bartel, D.P. (2009). MicroRNAs: target recognition and regulatory functions. Cell *136*, 215–233.

Braasch, D.A., Jensen, S., Liu, Y., Arar, K., White, M.A., and Corey, D.R. (2003). RNA interference in mammalian cells by chemically modified RNA. Biochemistry *42*, 7967–7975.

Calhoun, K.A., and Swartz, J.R. (2007). Energy systems for ATP regeneration in cell-free protein synthesis reactions. Methods Mol. Biol. *375*, 3–17.

Castel, S.E., and Martienssen, R.A. (2013). RNA interference in the nucleus: roles for small RNAs in transcription, epigenetics and beyond. Nat. Rev. Genet. *14*, 100–112.

Chu, Y., Yue, X., Younger, S.T., Janowski, B.A., and Corey, D.R. (2010). Involvement of argonaute proteins in gene silencing and activation by RNAs complementary to a non-coding transcript at the progesterone receptor promoter. Nucleic Acids Res. *38*, 7736–7748.

Daniels, S.M., and Gatignol, A. (2012). The multiple functions of TRBP, at the hub of cell responses to viruses, stress, and cancer. Microbiol. Mol. Biol. Rev. *76*, 652–666.

Dodd, D.W., Gagnon, K.T., and Corey, D.R. (2013). Digital quantitation of potential therapeutic target RNAs. Nucleic Acid Ther. *23*, 188–194.

Doyle, M., Badertscher, L., Jaskiewicz, L., Güttinger, S., Jurado, S., Hugenschmidt, T., Kutay, U., and Filipowicz, W. (2013). The double-stranded RNA binding domain of human Dicer functions as a nuclear localization signal. RNA *19*, 1238–1252.

Elbashir, S.M., Harborth, J., Lendeckel, W., Yalcin, A., Weber, K., and Tuschl, T. (2001). Duplexes of 21-nucleotide RNAs mediate RNA interference in cultured mammalian cells. Nature *411*, 494–498.

Gagnon, K.T., and Corey, D.R. (2012). Argonaute and the nuclear RNAs: new pathways for RNA-mediated control of gene expression. Nucleic Acid Ther. *22*, 3–16.

Gurtan, A.M., and Sharp, P.A. (2013). The role of miRNAs in regulating gene expression networks. J. Mol. Biol. *425*, 3582–3600. http://dx.doi.org/10.1016/j.jmb.2013.03.007.

Hammond, S.M., Bernstein, E., Beach, D., and Hannon, G.J. (2000). An RNA-directed nuclease mediates post-transcriptional gene silencing in Drosophila cells. Nature *404*, 293–296.

Harel-Bellan, A., Zazoua, M.A., Rachez, C., Muchardt, C., and Batsche, E. (2013). 10-million-years AGO: Argonaute on chromatin in yeast and human, a conserved mode of action? Transcription *4*. Published online April 12, 2013.

Hetzer, M.W. (2010). The nuclear envelope. Cold Spring Harb. Perspect. Biol. *2*, a000539.

Holding, C. (2004). RNAi active in the nucleus? Genome Biol. *6* http://dx.doi.org/10.1186/gb-spotlight-20050112-01.

Ikeda, K., Satoh, M., Pauley, K.M., Fritzler, M.J., Reeves, W.H., and Chan, E.K.L. (2006). Detection of the argonaute protein Ago2 and microRNAs in the RNA induced silencing complex (RISC) using a monoclonal antibody. J. Immunol. Methods *317*, 38–44.

Iwasaki, S., Kobayashi, M., Yoda, M., Sakaguchi, Y., Katsuma, S., Suzuki, T., and Tomari, Y. (2010). Hsc70/Hsp90 chaperone machinery mediates ATP-dependent RISC loading of small RNA duplexes. Mol. Cell *39*, 292–299.

Janowski, B.A., Younger, S.T., Hardy, D.B., Ram, R., Huffman, K.E., and Corey, D.R. (2007). Activating gene expression in mammalian cells with promoter-targeted duplex RNAs. Nat. Chem. Biol. *3*, 166–173.

Jeffries, C.D., Fried, H.M., and Perkins, D.O. (2011). Nuclear and cytoplasmic localization of neural stem cell microRNAs. RNA *17*, 675–686.

Katahira, J., and Yoneda, Y. (2011). Nucleocytoplasmic transport of microRNAs and related small RNAs. Traffic *12*, 1468–1474.

Katikireddy, K.R., and O'Sullivan, F. (2011). Immunohistochemical and immunofluorescence procedures for protein analysis. Methods Mol. Biol. *784*, 155–167.

Klouwen, H.M., and Appelman, A.W.M. (1967). Synthesis of adenosine triphosphate in isolated nuclei and intact cells. Biochem. J. *102*, 878–884.

Lazzaretti, D., Tournier, I., and Izaurralde, E. (2009). The C-terminal domains of human TNRC6A, TNRC6B, and TNRC6C silence bound transcripts independently of Argonaute proteins. RNA *15*, 1059–1066.

Li, L.C., Okino, S.T., Zhao, H., Pookot, D., Place, R.F., Urakami, S., Enokida, H., and Dahiya, R. (2006). Small dsRNAs induce transcriptional activation in human cells. Proc. Natl. Acad. Sci. USA *103*, 17337–17342.

Liao, J.Y., Ma, L.M., Guo, Y.H., Zhang, Y.C., Zhou, H., Shao, P., Chen, Y.Q., and Qu, L.H. (2010). Deep sequencing of human nuclear and cytoplasmic small RNAs reveals an unexpectedly complex subcellular distribution of miRNAs and tRNA 3′ trailers. PLoS ONE *5*, e10563.

Liu, J., Carmell, M.A., Rivas, F.V., Marsden, C.G., Thomson, J.M., Song, J.J., Hammond, S.M., Joshua-Tor, L., and Hannon, G.J. (2004). Argonaute2 is the catalytic engine of mammalian RNAi. Science *305*, 1437–1441.

Liu, Y., Ye, X., Jiang, F., Liang, C., Chen, D., Peng, J., Kinch, L.N., Grishin, N.V., and Liu, Q. (2009). C3PO, an endoribonuclease that promotes RNAi by facilitating RISC activation. Science *325*, 750–753.

Liu, J., Hu, J., and Corey, D.R. (2012). Expanding the action of duplex RNAs into the nucleus: redirecting alternative splicing. Nucleic Acids Res. *40*, 1240–1250.

Ma, E., Zhou, K., Kidwell, M.A., and Doudna, J.A. (2012). Coordinated activities of human dicer domains in regulatory RNA processing. J. Mol. Biol. *422*, 466–476.

MacRae, I.J., Ma, E., Zhou, M., Robinson, C.V., and Doudna, J.A. (2008). In vitro reconstitution of the human RISC-loading complex. Proc. Natl. Acad. Sci. USA *105*, 512–517.

Malone, C.D., and Hannon, G.J. (2009). Small RNAs as guardians of the genome. Cell *136*, 656–668.

Martinez, N.J., Chang, H.M., Borrajo, Jde.R., and Gregory, R.I. (2013). The co-chaperones Fkbp4/5 control Argonaute2 expression and facilitate RISC assembly. RNA *19*, 1583–1593.

Matranga, C., Tomari, Y., Shin, C., Bartel, D.P., and Zamore, P.D. (2005). Passenger-strand cleavage facilitates assembly of siRNA into Ago2-containing RNAi enzyme complexes. Cell *123*, 607–620.

Matsui, M., Zhang, H., Chu, Y., Gagnon, K.T., Shaikh, S., Kuchimanchi, S., Manoharan, M., Corey, D.R., and Janowski, B.A. (2013). Promoter RNA links transcriptional regulation of inflammatory pathway genes. Nucleic Acids Res. *41*, 10086–10109.

Meister, G., Landthaler, M., Patkaniowska, A., Dorsett, Y., Teng, G., and Tuschl, T. (2004). Human Argonaute2 mediates RNA cleavage targeted by miRNAs and siRNAs. Mol. Cell *15*, 185–197.

Michelsen, U., and von Hagen, J. (2009). Isolation of subcellular organelles and structures. Methods Enzymol. *463*, 305–328.

Morris, K.V., Chan, S.W., Jacobsen, S.E., and Looney, D.J. (2004). Small interfering RNA-induced transcriptional gene silencing in human cells. Science *305*, 1289–1292.

Ohrt, T., Mütze, J., Staroske, W., Weinmann, L., Höck, J., Crell, K., Meister, G., and Schwille, P. (2008). Fluorescence correlation spectroscopy and fluorescence cross-correlation spectroscopy reveal the cytoplasmic origination of loaded nuclear RISC in vivo in human cells. Nucleic Acids Res. *36*, 6439–6449.

Ohrt, T., Muetze, J., Svoboda, P., and Schwille, P. (2012). Intracellular localization and routing of miRNA and RNAi pathway components. Curr. Top. Med. Chem. *12*, 79–88.

Pare, J.M., LaPointe, P., and Hobman, T.C. (2013). Hsp90 cochaperones p23 and FKBP4 physically interact with hAgo2 and activate RNA interference-mediated silencing in mammalian cells. Mol. Biol. Cell *24*, 2303–2310.

Rivas, F.V., Tolia, N.H., Song, J.J., Aragon, J.P., Liu, J., Hannon, G.J., and Joshua-Tor, L. (2005). Purified Argonaute2 and an siRNA form recombinant human RISC. Nat. Struct. Mol. Biol. *12*, 340–349.

Robb, G.B., Brown, K.M., Khurana, J., and Rana, T.M. (2005). Specific and potent RNAi in the nucleus of human cells. Nat. Struct. Mol. Biol. *12*, 133–137.

Rüdel, S., Flatley, A., Weinmann, L., Kremmer, E., and Meister, G. (2008). A multifunctional human Argonaute2-specific monoclonal antibody. RNA *14*, 1244–1253.

Shaw, P.J. (2006). Comparison of widefield/deconvolution and confocal microscopy for three-dimensional imaging. In Handbook of Biological Confocal Microscopy, J.B. Pawley, ed. (New York: Springer), pp. 453–467.

Spector, D.L. (2011). Immunofluorescence localization of nuclear proteins. Cold Spring Harb. Protoc. *2011*, 1276–1280.

Stalder, L., Heusermann, W., Sokol, L., Trojer, D., Wirz, J., Hean, J., Fritzsche, A., Aeschimann, F., Pfanzagl, V., Basselet, P., et al. (2013). The rough endoplasmatic reticulum is a central nucleation site of siRNA-mediated RNA silencing. EMBO J. *32*, 1115–1127.

Till, S., Lejeune, E., Thermann, R., Bortfeld, M., Hothorn, M., Enderle, D., Heinrich, C., Hentze, M.W., and Ladurner, A.G. (2007). A conserved motif in Argonaute-interacting proteins mediates functional interactions through the Argonaute PIWI domain. Nat. Struct. Mol. Biol. *14*, 897–903.

Valencia-Sanchez, M.A., Liu, J., Hannon, G.J., and Parker, R. (2006). Control of translation and mRNA degradation by miRNAs and siRNAs. Genes Dev. *20*, 515–524.

Vickers, T.A., Koo, S., Bennett, C.F., Crooke, S.T., Dean, N.M., and Baker, B.F. (2003). Efficient reduction of target RNAs by small interfering RNA and RNase H-dependent antisense agents. A comparative analysis. J. Biol. Chem. *278*, 7108–7118.

Wang, Y., Juranek, S., Li, H., Sheng, G., Tuschl, T., and Patel, D.J. (2008). Structure of an argonaute silencing complex with a seed-containing guide DNA and target RNA duplex. Nature *456*, 921–926.

Weinmann, L., Höck, J., Ivacevic, T., Ohrt, T., Mütze, J., Schwille, P., Kremmer, E., Benes, V., Urlaub, H., and Meister, G. (2009). Importin 8 is a gene silencing factor that targets argonaute proteins to distinct mRNAs. Cell *136*, 496–507.

Wilson, R.C., and Doudna, J.A. (2013). Molecular mechanisms of RNA interference. Annu. Rev. Biophys. *42*, 217–239.

Wuarin, J., and Schibler, U. (1994). Physical isolation of nascent RNA chains transcribed by RNA polymerase II: evidence for cotranscriptional splicing. Mol. Cell. Biol. *14*, 7219–7225.

Ye, X., Huang, N., Liu, Y., Paroo, Z., Huerta, C., Li, P., Chen, S., Liu, Q., and Zhang, H. (2011). Structure of C3PO and mechanism of human RISC activation. Nat. Struct. Mol. Biol. *18*, 650–657.

Zamore, P.D., Tuschl, T., Sharp, P.A., and Bartel, D.P. (2000). RNAi: double-stranded RNA directs the ATP-dependent cleavage of mRNA at 21 to 23 nucleotide intervals. Cell *101*, 25–33.

Zeng, Y., and Cullen, B.R. (2002). RNA interference in human cells is restricted to the cytoplasm. RNA *8*, 855–860.

RNAi Factors are Present and Active in Human Cell Nuclei

Keith T. Gagnon*, Liande Li*, Yongjun Chu, Bethany A. Janowski, and David R. Corey

Departments of Pharmacology and Biochemistry, University of Texas Southwestern Medical Center, Dallas, Texas, 75390-9041.

*These authors contributed equally.

SUPPLEMENTAL INFORMATION

SUPPLEMENTAL EXPERIMENTAL PROCEDURES

Tissue culture and siRNA transfection

HeLa cells were cultured in Dulbecco's Modified Eagle's Medium (DMEM) supplemented with 5% fetal bovine serum (FBS) and 0.5% non-essential amino acids (NEAA). T47D cells (ATCC) were cultured in RPMI medium supplemented with 10% FBS, 0.5% NEAA, 20 μg/mL insulin, 10 mM pH 7.0-7.6 HEPES, and 1 mM sodium pyruvate. Fibroblast cells (Coriell Institute, GM04281) were cultured in minimum essential medium (MEM) supplemented with 10% FBS and 0.5% NEAA. A549 cells (ATCC) were cultured in F-12K medium supplemented with 10% FBS. T47D cells stably expressing FLAG-HA-tagged Ago2 were cultured identically to T47D cells but media supplemented with 0.2 mg/mL G418. All cells were grown at 37°C in 5% CO_2.

Lipofectamine RNAiMAX (Invitrogen) was used to deliver siRNAs into HeLa cells following the manufacturer's recommended protocol in OptiMEM low serum medium (Invitrogen). Growth media was changed to full medium after 24 h. Transfected cells were harvested 72 h after transfection for qPCR and RACE analyses, 36 h after transfection for in vitro Ago2 cleavage assays, and 48 h after transfection for FISH analysis. Sequences of siRNAs used are listed in Table S1.

Nuclear and cytoplasmic cell fractions

Cells were harvested with trypsin-EDTA solution (Invitrogen), washed with PBS then resuspended in ice-cold hypotonic lysis buffer (HLB) (10 mM Tris-HCl, pH 7.5, 10 mM NaCl, 3 mM $MgCl_2$, 0.3% NP-40) supplemented with 1% Protease Inhibitor Cocktail Set I (Calbiochem), 1 mM sodium fluoride and 1 mM sodium orthovanadate at a final of 1 mL/75 mg wet cell pellet. After incubation on ice for 15 min and gentle pipetting, lysate was spun at

4°C at 800xg for 5 min. The supernatant was kept as cytoplasmic extract and NaCl and glycerol were added to a final of 140 mM and 10%, respectively. Pelleted nuclei were washed 3x with ice-cold HLB by 5 min incubation on ice, pipetting and vortexing, then spinning at 4°C at 100-200xg for 2 min. For nuclear extracts, nuclei were resuspended in ice-cold nuclear lysis buffer (NLB) (20 mM Tris-HCl, pH 7.5, 0.15 M NaCl, 3 mM $MgCl_2$, 0.3% NP-40, 10% glycerol) supplemented with 1% Protease Inhibitor Cocktail Set I, 1 mM sodium fluoride and 1 mM sodium orthovanadate at a final of 0.5 mL/75 mg of original wet cell pellet weight (1/2 the volume of cytoplasmic fraction). Nuclei were sonicated on ice at 20% power 3x for 15 sec in 4 mL volumes. After high speed centrifugation at 4°C for 15 min to remove insoluble cell debris, the soluble fraction was kept as nuclear extract. All extracts were aliquoted, flash-frozen in liquid nitrogen, then stored at -80°C for later use. Prior to use, extracts were spun again or filtered through 0.45 µm filter units.

Optimization of nuclei isolation protocol

A protocol similar to the above described for nuclear and cytoplasmic fraction preparation was followed except detergent was either omitted or TWEEN-20, NP-40 or Triton X-100 non-ionic detergents were included in HLB at the indicated concentrations. After the final nuclei wash, a fraction of the nuclei were aliquoted for visualization by fluorescence microscopy while the remaining nuclei were resuspended in NLB and sonicated to prepare nuclear extracts as described above. Nuclei were prepared for microscopy by washing 1x in ice-cold PBS then incubating in PBS + 1 µM ER Tracker Red (Invitrogen) for 20 min on ice. Nuclei were washed in ice-cold PBS then diluted 10-fold in ice-cold PBS + 4% paraformaldahyde and incubated on ice 10 min. Nuclei were resuspended by pipetting and spotted on glass slides. After partial air-drying, one drop of Vectashield Hard Set Mounting Medium with DAPI

(Vector Laboratories, H-1500) was added, a coverslip added and mounting media allowed to harden at room temperature for 15 min.

Nuclei were visualized with a 60x objective lens and DAPI and TRITC filters on a wide-field epifluorescence Deltavision microscope. Z-sections were taken at 0.15 μm thickness. Images were deconvoluted by blind deconvolution using AutoQuant X3 (Media Cybernetics), stacked and ER tracker staining pseudo-colored yellow in ImageJ for visualization.

Western blot analysis

Cell extracts were prepared as described above. For comparing nuclear and cytoplasmic fractions by Western blot, the same cell equivalents of extract were separated by electrophoresis (1/2 the volume of nuclear extract for every 1 volume of cytoplasmic). In general, loading equal amounts of total protein is unsatisfactory for comparing the nuclear and cytoplasmic levels of specific proteins since there is approximately 4-fold more total protein in cytoplasmic extracts. Protein was separated on 4-20% gradient SDS-PAGE TGX pre-cast gels (Biorad) at 100 V for 75 min. After gel electrophoresis, proteins were transferred to nitrocellulose membrane (Hybond-C Extra, GE Healthcare Life Sciences) at 100 V for 90 min. Membranes were blocked for 30 min at room temperature with 5% milk protein in PBS + 0.05% TWEEN-20 (PBST).

Blocked membranes were incubated with the following specific primary antibodies for 16 h at 4°C in PBST + 5% milk with rocking: anti-Ago2 at 1:1000 (Abcam, ab57113), anti-TNRC6A at 1:4000 (Bethyl Laboratories, A302-329A) or anti-TNRC6A at 1:3000 (kind gift from Edward Chan, Univ. Florida, rb5182), anti-Dicer at 1:1000 (Abcam, ab14601), anti-TRBP at 1:1000 (Abcam, ab72110) or anti-TRBP at 1:3000 (kind gift from Qinghua Liu lab); anti-Calreticulin at 1:1500 (Cell Signaling, 2891S), anti-Calnexin at 1:1500 (Cell Signaling,

2433S), anti-Histone H3 at 1:10000 (Abcam, ab1791), anti-Lamin A/C at 1:1500 (Abcam, ab8984), anti-OxPhos at 1:1000 (Invitrogen, A21351), anti-tubulin at 1:6000 (Sigma-Aldrich, T5201), anti-Ago1 at 1:1000 (Wako Chemical, 015-22411), anti-Ago3 at 1:500 (Active Motif, 39788); anti-Ago4 at 1:500 (Active Motif, 39856), anti-PACT at 1:1000 (Abcam, ab75749), anti-Hsp90 at 1:500 (Enzo Life Sci., ADI-SPA-830-D), anti-Hsc70 at 1:500 (Enzo Life Sci., ADI-SPA-810-D), anti-Aha1 at 1:1000 (Abcam, ab56721), anti-FKBP4 at 1:50000 (Abcam, ab124906), anti-Cdc37 at 1:50000 (Abcam, ab108305), anti-p23 at 1:1000 (Abcam, ab2814).

After primary antibody incubation, membranes were washed 3x for 5 min at room temperature with PBST then incubated for 30-45 min at room temperature with HRP-conjugated anti-mouse at 1:10000 (Jackson Laboratories, 715-035-150) or anti-rabbit at 1:5000 (Jackson Laboratories, 711-035-152) in PBST + 5% milk. Membranes were washed again 3x for 15 min in PBST at room temperature, then protein bands visualized using SuperSignal West Pico Chemiluminescent Substrate (Thermo Scientific). For quantification of RNAi factor protein levels from Western blots of cellular fractions, films were scanned and bands quantified using ImageJ.

Co-immunoprecipitation

Co-immunoprecipitation experiments were performed by mixing 40 µl of Protein G Plus/Protein A resin (Calbiochem), 2 µg of antibody and nuclear extract (~0.5-1 mg total protein, precleared at 4°C for 30 min using ~15 µL Protein G Plus/Protein A resin and ~0.3 µg of corresponding IgG) and rotating at 4°C for 2-3 h. Resin was washed 4x with IP wash buffer (20 mM Tris-HCl, pH 7.5, 0.4 M NaCl, 2 mM $MgCl_2$, 0.05% NP-40, 0.025% SDS) and co-purified proteins eluted by boiling resin in 25 µl 1x SDS loading buffer. Eluted protein was resolved by SDS-PAGE and proteins detected by Western blot as described above. When

indicated, 20 µg of RNase A was added before incubation. For FLAG-tagged Ago2 co-immunoprecipitation, about 20 µL ANTI-FLAG-M2 affinity gel (Sigma) and nuclear extract from T47D cells stably expressing FLAG-HA-tagged Ago2 (~0.5-1 mg total protein) were rotated at 4°C for ~1.5-2.5 h, followed by washing and elution as described above.

Chromatographic and ammonium sulfate fractionation of cell extracts

Nuclear extracts were prepared as described above but concentrated 2-fold by using 1/2 the standard amount of NLB during nuclei resuspension and sonication. For size-exclusion chromatography, 2 mL of nuclear extract was either treated with 50 µg of RNase A or 200 units of SUPERase-In (Ambion) for 1 h at room temperature. Samples were then spun down at high speed and 0.45 µm filtered and injected onto a Superdex 200 HiLoad 16/60 FPLC column (Amersham Pharmacia) that was pre-equilibrated with FPLC buffer (20 mM Tris-HCl, pH 7.5, 150 mM NaCl, 3 mM $MgCl_2$, 5% glycerol). Protein was eluted off the column with FPLC buffer and the elution collected in fractions at 4°C that were then snap-frozen in liquid nitrogen and stored at -80°C. Western blot analysis of fractions was performed as described above. For subsequent tandem fractionation by anion exchange, size-exclusion fractions were concentrated 3-fold and diluted to 0.1 M NaCl and injected onto a Mono-Q FPLC column (Amersham Pharmacia) equilibrated with FPLC buffer at 0.1 M NaCl. Elution was performed at room temperature with a linear gradient from 0.1 to 1 M NaCl in FPLC buffer. Fractions were collected and snap-frozen in liquid nitrogen. Western blot analysis was performed as described above.

Ammonium sulfate cuts were performed by addition of saturated ammonium sulfate solution to the extract up to the indicated final percentage and incubated on ice for 15 min. Precipitated protein was pelleted by centrifugation at 18,000xg for 20 min at 4°C. Supernatant

was kept and additional ammonium sulfate added up to the next indicated percentage and incubation and centrifugation repeated. Precipitated protein pellets were resuspended in identical volumes of SDS loading buffer, resolved by SDS-PAGE and probed by Western blot as described above.

Analysis of siRNA-mediated RNA knock-down in cellular compartments

HeLa cells were transfected in quadruplicate with 25 nM siRNA then harvested 72 h later with trypsin-EDTA solution. Cells were washed with PBS then counted with a hemocytometer. Five million cells were aliquoted and resuspended in 380 µL of ice-cold hypotonic lysis bufer (HLB) (10 mM Tris, pH 7.5, 10 mM NaCl, 3 mM $MgCl_2$, 0.3% NP-40) and incubated on ice for 15 min. Lysate was pipetted and spun at 500xg at 4°C for 5 min. Supernatant was kept as cytoplasmic fraction, 40 µL of 3 M sodium acetate, pH 5.5, added, 100% ethanol added up to 70%, and precipitated at -20°C overnight.

Pelleted nuclei were washed 3x with ice-cold HLB and pipetting and vortexing then resuspended in 380 µL of ice-cold modified Wuarin-Schibler buffer (MWS) (10 mM Tris-HCl, pH 7.0, 4 mM EDTA, 0.3 M NaCl, 1 M urea, 1% NP-40) (Wuarin and Schibler, 1994). Sample was incubated on ice for 30 min. with vortexing every 10 min., then spun at 500xg at 4°C for 5 min. Supernatant was kept as nucleoplasmic fraction, 40 µL of 3 M sodium acetate, pH 5.5, added, 100% ethanol added up to 70%, and precipitated at -20°C overnight.

Pelleted chromatin was washed 3x with ice-cold MWS then 1 mL Trizol (Invitrogen) was added to the final chromatin pellet. To process cytoplasmic and nucleoplasmic fractions, precipitates were pelleted at 18000xg for 15 min at 4°C then 1 mL Trizol added to each pellet. Samples in Trizol were heated to 70°C with vortexing until completely dissolved (5-10 min), then cooled to room temperature. To each sample 0.2 mL chloroform:isoamyl alcohol (24:1)

was added, samples vortexed, then spun at 18000xg for 10 min. The top aqueous layer was collected and RNA precipitated by addition of 1 volume of isopropanol and incubation at -20°C overnight. RNA was pelleted by spinning at 18000xg, washed with 70% ethanol, then air dried and prepared for quantitative PCR or 5' RACE.

Quantitative PCR

Identical volumes of RNA (representing approximately the same number of cells and ranging from 1-2 µg of RNA) that were prepared from cellular fractions above were treated with 2 units of DNase I (Worthington) in 9.5 µL of DNase I buffer (10 mM Tris-HCl, pH 7.0, 10 mM NaCl, 2 mM $MgCl_2$, 0.5 mM $CaCl_2$) for 15 min at room temperature to degrade any genomic DNA contamination. Afterwards, 0.5 µL of a 50 mM EDTA, 10 mM EGTA solution was added and DNase I heat-inactivated at 70°C for 10 min. Treated RNAs were reverse-transcribed using the High Capacity cDNA Reverse Transcription Kit (Applied Biosystems) in a final volume of 20 µL. Quantitative PCR (qPCR) was performed using iTaq Supermix with ROX (Biorad) with ~10-20 ng of cDNA as template.

Data were normalized relative to measured GAPDH levels in each cellular compartment. Because no normalization control exists that is the same level across cellular compartments, and because spike-in controls can have variability in performance (data not shown), comparisons among treatments were only performed within each cellular compartment and not across cellular compartments (ie. chromatin to chromatin, not cytoplasm to chromatin). Primers used in qPCR are listed in Table S1.

Rapid Amplification of cDNA Ends (RACE)

RACE was performed using the GeneRacer Kit (Invitrogen) following the manufacturer's recommended protocol. cDNA was prepared from ~1 µg RNA from each cellular fraction (DNase-treated and prepared as described above) by reverse-transcription (RT) reaction using random primers. The 5' end of cDNA was amplified using Platinum Taq DNA polymerase (Invitrogen) and specific primer sets for Malat1 and RPL30 (Table S1). The thermal cycling condition was 94°C for 2 min, followed by 5 cycles of 94°C for 30 sec and 72°C for 1 min, 5 cycles of 94°C for 30 sec and 70°C for 1 min, and 25 cycles of 94°C for 30 sec, 65-66°C for 30 sec, and 68°C for 1 min, followed by final extension of 68°C for 10 min. PCR products were analyzed on 1.2-1.5% agarose gel (Fig. S6B-C). Major PCR products on gels were excised and cloned into pCR 4-TOPO vectors, transformed into TOP10 chemically competent cells, then sequenced to map the 5' cleavage sites. Chromatin-associated cleavage products for RPL30 were below our detection limit (Fig. S6C), despite performing nested PCR with multiple primer sets (data not shown). This result may reflect the relatively low level of RPL30 mRNA actually associated with chromatin. In addition to relative starting levels of targeted RNA, detection of cleavage products will also depend upon other factors like the rate of cleavage product formation and degradation.

In vitro Ago2 cleavage assay

HeLa cells were either untreated or transfected with 25 nM siLuc or siLuc_mm (see Table S1) then harvested 36 h later and nuclear and cytoplasmic extracts prepared as described above. Ago2 protein was immunoprecipitated using 1.5 µg anti-Ago2 antibody (Abcam, ab57113), 30 µL Protein G Plus/Protein A agarose (Calbiochem) and 200 µL extract with rocking at room temperature for 1 h. Resin was washed 3x with 0.5 mL $IPWB_{500}$ (20 mM Tris-HCl, pH 7.5, 4 mM $MgCl_2$, 0.5 M NaCl, 0.05% NP-40) then 1x with 0.5 mL IPDB (20 mM Tris-HCl, pH 7.5, 3

mM $MgCl_2$, 0.15 M NaCl) at room temperature. Synthesized target RNA substrate was 5' radiolabeled with T4 polynucleotide kinase and $[\gamma]^{32}$P-ATP, then gel-purified. Labeled target RNA substrate (50,000 cpms, ~0.1 pmols) was added to the washed Ago2-bound resin in 20 µL 1X RNAi buffer (20 mM Tris-HCl, pH 7.5, 4 mM $MgCl_2$, 0.5 mM DTT, 80 mM NaCl, 20 mM KCl, 0.5 mM EDTA) supplemented with 1 mg/mL yeast tRNA, 20 units SUPERase-In (Ambion), and 0.5 mM ATP.

Reactions were incubated at 30°C for 1.5 hr with periodic mixing and RNA collected by addition of 0.5 µL of 0.5 M EDTA then phenol extracted. Extracted RNA was precipitated with 9 volumes of 2% $LiClO_4$ in acetone, washed with acetone, resuspended in 90% formamide, 1x Tris-Borate EDTA (TBE) buffer, boiled for 3 min, then resolved on a 15% denaturing polyacrylamide (7 M urea, 1x TBE, 2% glycerol) sequencing gel. The gel was dried and exposed to a phosphorimager screen overnight to visualize radioactive bands. Target RNA substrate consists of a single siLuc siRNA target site flanked by firefly luciferase gene sequence and capped with two terminal DNA bases on each end. Target RNA substrate sequence (DNA bases capitalized, complementary siRNA target site in brackets):

GAacaauugauuuuacagac[gcacauaucgaggugaaca]ucacguacgcggaauacuTC.

Synthetic product RNA sequence: GAacaauugauuuuacagac[gcacauauc.

Immuno-fluorescence and co-localization analysis

Immuno-fluorescence was performed similarly to that previously described (Ohrt et al., 2012; Spector, 2011) with modifications. Briefly, cells were grown for 16-24 h to 50-70% confluency on 35 mm dishes (MatTek Corporation, P35GCOL-1.5-14-C) with a 14 mm glass bottom of 1.5 mm thickness. Cells were washed with PBS then fixed in freshly made 2% formaldehyde in PBS or 4% paraformaldehyde in PBS for 15 min at 20°C, or in 70% ethanol for at least 30

min at 4°C. Fixed cells were washed 3x in PBS for 10 min at 4°C. Cells were permeabilized in PBS containing 0.2% Triton X-100 and 1% normal goat serum (NGS) for 5-10 min on ice then washed 3x with ice-cold PBS + 1% NGS at 4°C for 10 min.

The cells were incubated in primary antibody for 1 hr at room temperature or overnight at 4°C. Primary antibodies were diluted in PBS + 1% NGS and incubated for 1 h at room temperature or at 4°C overnight: anti-Ago2 at 1:100 (Abcam, ab57113), anti-Ago2 at 1:50 or 1:100 (Sigma-Aldrich, clone 11A9, SAB4200085), anti-Ago2 at 1:50 or 1:100 (Wako Chemicals, 015-22031), anti-TNRC6A at 1:50 or 1:100 (Bethyl Laboratories, A302-329A), anti-Dicer at 1:100 (Abcam, ab14601), anti-TRBP at 1:100 (Abcam, ab72110). Cells were washed 3x in PBS + 1% NGS for 10 min at room temperature, then incubated in 4 µg/mL secondary antibody diluted in PBS + 1% NGS for 1 h at room temperature. Secondary antibodies were Alexa Fluor 488 Goat Anti-Mouse IgG (Invitrogen, A-11001), Alexa Fluor 594 Goat Anti-Rabbit IgG (Invitrogen, A-11012), and Alexa 594 Goat Anti-Rat IgG (Invitrogen, A-11007). Cells were washed 4x in PBS for 10 min at room temperature then Vectashield Hard Set Mounting Medium with DAPI (Vector Laboratories, H-1500) was added to the cells then covered with a coverslip and allowed to harden for 15 min at room temperature.

Cells were imaged with a 60x objective lens and DAPI, FITC and TRITC filters on a wide-field epifluorescence Deltavision deconvolution microscope. Z-sections were taken at 0.1, 0.15 or 0.2 µm for at least 6 µm thickness. Images were blind deconvoluted using AutoQuant X3 (Media Cybernetics) and stacked and analyzed in Imaris (Bitplane). Alternatively, some samples were imaged by Andor spin disc confocal microscopy. The Co-localization channel of Ago2 (FITC, green) and TNRC6A (TRITC, red) was calculated using Imaris software based on the correlation of the strength of linear relation between the red

channel and the green channel and the threshold levels for calculation of co-localization were selected above background signals.

Fluorescence *in situ* hybridization (FISH)

Cells were grown for 16-24hrs to 50-70% confluence on 35mm MatTek dishes as described for immuno-fluorescence above. Cells were transfected with 25 nM siLuc or siMalat1 as described above. At 48 h post transfection, cells were washed with PBS and fixed in ice-cold 4% paraformaldehyde in PBS for 15 min at 20°C, followed by permeabilization in 70% ethanol for at least 30 min at 4°C.

From this point forward, the protocol recommended by the manufacturer of the FISH probes for Malat-1 (Biosearch Technologies, New Stellaris RNA FISH Probe for Malat-1, SMF-2035-1) was followed with modifications. Briefly, cells were washed with 1 mL of wash buffer (10% formamide in 2x SSC) and incubated 5 min at room temperature, then incubated in hybridization buffer (10% formamide, 2x SSC, 100 mg/mL dextran sulfate, 1 mM vanadyl ribonucleoside complex) containing Malat-1 probe (125 nM) in a humidified chamber at 37°C for 4-16 h in the dark. Cells were washed 1x with wash buffer in the dark at 37°C for 30 min. Vectashield Hard Set Mounting Medium with DAPI (Vector Laboratories, H-1500) was then added, covered with a coverslip and allowed to harden for 15 min at room temperature. Cells were imaged and analyzed the same as described above for immuno-fluorescence but using DAPI and Cy-5 filters. Z-stacks were taken with 0.15 or 0.2 μm slices and 6 μm thickness.

Small RNA-seq library preparation and sequencing

For whole cell small RNA sequencing, T47D cells were harvested and then dissolved in TRIzol (Sigma). For sequencing of small RNA from cell nuclei, pure nuclei were isolated first

as described above. Nuclei were then dissolved in TRIzol. Small RNA was isolated using miRNeasy Mini Kit (Qiagen) and then treated with DNase I (Worthington) for 20 min at 37°C to remove any contaminating genomic DNA. The small RNA-seq library was made using Illumina Small RNA Truseq kit following the manufacturer's recommended protocol. RNA-seq libraries were sequenced on a Illumina HiSeq 2000 as per manufacturer's instructions for single-end 1x50. Approximately, 30 million raw reads (averaged over two replicates) were obtained per sample. Reads with low quality score were removed and reads that passed the filtration were trimmed by removing the adaptor sequence. Trimmed reads shorter than 15 nt were also excluded from analysis. Filtered and trimmed reads were aligned to the human genome (hg19) using Bowtie2 by allowing up to two mismatches to the reference sequence. Up to 10 different alignments per read were permitted. For reads that were aligned to multiple positions in the reference genome, the single aligned read with the fewest mismatches was selected using a Perl script. If multiple reads still remained, the original read would be disregarded. Approximately 70% of raw reads were successfully aligned. Finally, the aligned reads were again mapped to the UCSC miRNA database and miRBase (mature miRNAs) to search for possible miRNA hits.

Sequencing of AGO2-associated small RNA in cell nuclei

RNA Immunoprecipitation (RIP) assay using nuclear lysate (T47D cells) was performed as described (Chu et al., 2010; Matsui et al., 2013) using anti-human Ago2 antibody (Wako Chemical, 015-22031). A non-specific mouse IgG antibody was used as a control. The isolated RNA was loaded on a 10% polyacrylamide gel and the small RNA fraction (15nt-40nt) was cut out and extracted. The small RNA was then subjected to polyadenylation by using a poly(A) tailing kit (Ambion). 3'-deoxy-ATP (cordycepin triphosphate, Jena

Biosciences) was introduced 10 min after the initiation of the polyadenylation reaction for 3'-end blocking and tail length limitation (performed by Helicos, Inc.). The Direct RNA Sequencing (DRS) was carried out on a single molecule Helicos sequencer. Raw sequencing data was filtered to remove low quality reads and subsequently aligned using the Helisphere package, a software designed to specifically analyze sequencing data generated from the Helicos sequencer. The aligned reads were again mapped to the UCSC miRNA database and miRBase (mature miRNAs) to search for possible miRNA hits.

In vitro Dicer processing assay

Dicer was immunoprecipitated using 3 µg of anti-Dicer (Abcam, ab14601) antibody (or 3 µg normal mouse IgG as control), 50 µL Protein G Plus/Protein A agarose (Calbiochem) and 200 µL of HeLa nuclear or cytoplasmic extract (prepared as described above) with rotation at room temperature for 1 h. Resin was washed 3x with 0.5 mL $IPWB_{300}$ (20 mM Tris-HCl, pH 7.5, 4 mM $MgCl_2$, 0.3 M NaCl, 0.05% NP-40) then 1x with 0.5 mL IPDB (20 mM Tris-HCl, pH 7.5, 3 mM $MgCl_2$, 0.15 M NaCl) at room temperature. Pre-miR-19a substrate was *in vitro* transcribed in the presence of $[\alpha]^{32}$P-ATP then gel-purified. Radiolabeled pre-miR-19a RNA (50,000 cpms) was added to the washed Dicer-bound resin in 20 µL 1X Dicer assay buffer (40 mM Tris-HCl, pH 7, 3 mM $MgCl_2$, 50 mM NaCl) supplemented with 2 mM ATP and 200 units SUPERase-In (Ambion).

Reactions were incubated at 32°C for 1 hr with periodic mixing and RNA collected by addition of 0.5 µL of 0.5 M EDTA and 5 µg yeast tRNA then phenol extracted. Extracted RNA was precipitated with 9 volumes of 2% $LiClO_4$ in acetone, washed with acetone, resuspended in 90% formamide, 1x Tris-Borate EDTA (TBE) buffer, boiled for 3 min, then resolved on a 15% denaturing polyacrylamide (7 M urea, 1x TBE, 2% glycerol) sequencing gel. The gel was

dried and exposed to a phosphorimager screen overnight to visualize radioactive bands. Pre-miR-19a sequence from miRBase was used prepare *in vitro* transcription template. DNA seqeunces below were annealed and used for *in vitro* transcription (Epicentre Ampliscribe T7 In Vitro Transcription Kit) following the manufacturers protocol.

hsa-miR-19a pre-miRNA T7 sense (lowercase = T7 promoter):

ctaatacgactcactataGCAGTCCTCTGTTAGTTTTGCATAGTTGCACTACAAGAAGAATGTAGT
TGTGCAAATCTATGCAAAACTGATGGTGGCCTGC

hsa-miR-19a pre-miRNA T7 antisense (lowercase = T7 promoter):

GCAGGCCACCATCAGTTTTGCATAGATTTGCACAACTACATTCTTCTTGTAGTGCAACTA
TGCAAAACTAACAGAGGACTGCtatagtgagtcgtattag

In vitro Ago2 small RNA loading assay

Duplex siRNA or single-strand guide RNA radiolabeled at the 5' end was incubated with cell extracts supplemented with 1 mM ATP for 1 h at room temperature with rotation. For reactions using mismatch-containing siLuc, the standard antisense siLuc strand was radiolabeled and annealed to sense strand with the indicated base position mismatches (see Table S1) then gel-purified before use. When indicated, phosphocreatine (10 mM) and creatine kinase (100 µg/mL) were added as an ATP regeneration system. Ago2 was immunoprecipitated using 2µg of anti-Ago2 antibody (Abcam, ab57113) and 40 µL of Protein G Plus/Protein A agarose (Calbiochem) with rotation for 1 h at room temperature. Resin was washed 3x with 0.8 mL $IPWB_{500}$ (20 mM Tris-HCl, pH 7.5, 4 mM $MgCl_2$, 0.5 M NaCl, 0.05% NP-40) and 1x with 0.5 mL IPDB (20 mM Tris-HCl, pH 7.5, 3 mM $MgCl_2$, 0.15 M NaCl) at room temperature. Co-precipitated RNA was collected by addition of 0.5 µL of 0.5 M EDTA and 5 µg yeast tRNA then phenol-chloroform extraction. Extracted RNA was precipitated with

9 volumes of 2% $LiClO_4$ in acetone, washed with acetone, resuspended in 90% formamide, 1x Tris-Borate EDTA (TBE) buffer, boiled for 3 min, then resolved on a 15% denaturing polyacrylamide (7M urea, 1x TBE, 2% glycerol) sequencing gel. The gel was dried and exposed to a phosphorimager screen overnight to visualize radioactive bands.

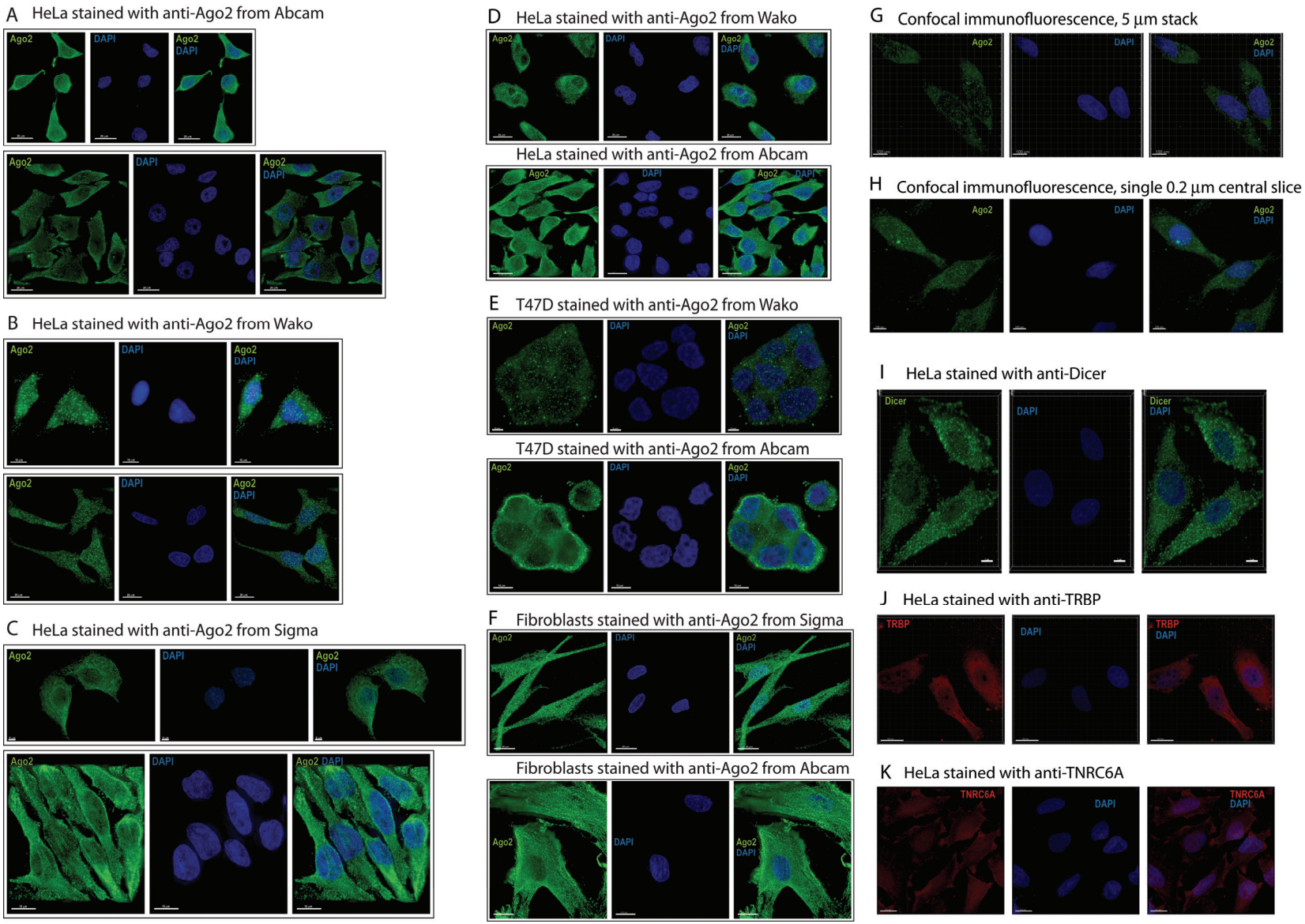

<u>Figure S1, Related to Figure 1</u>: Staining of Ago2 and other RNAi factors is observed in the nucleus of multiple human cell lines with multiple antibodies. Cells were fixed, permeabilized and immuno-stained identically except for the use of different primary and secondary antibodies (see Methods). (**A-C**) HeLa stained with anti-Ago2 from Abcam, Wako or Sigma-Aldrich and imaged by wide-field epi-immunofluorescence microscopy with blind deconvolution. Z-stacks are 5 µM thick for all images. (**D-F**) HeLa, T47D or fibroblast cells stained with anti-Ago2 from Abcam, Wako, or Sigma-Aldrich and imaged by wide-field epi-immunofluorescence microscopy with blind deconvolution. Z-stacks are 5 µM thick for all images. (**G-H**) HeLa cells stained with anti-Ago2 from Abcam and imaged by spinning disc confocal immunofluorescence microscopy. (**I-K**) HeLa cells stained with anti-Dicer, anti-TRNC6A, or anti-TRBP and imaged by wide-field epi-immunofluorescence microscopy with blind deconvolution. Z-stacks are 6 µm thick (panel I), 4 µm thick (panel J), and 6 µm thick (panel K).

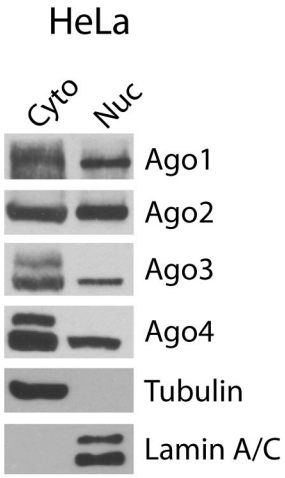

Figure S2, Related to Figure 2: Argonaute family proteins are detected in HeLa nuclear extracts by Western blot. Cell extracts were prepared as described and probed by Western blot with specific antibodies to detect each Ago family protein, Ago1, Ago2, Ago3 and Ago4.

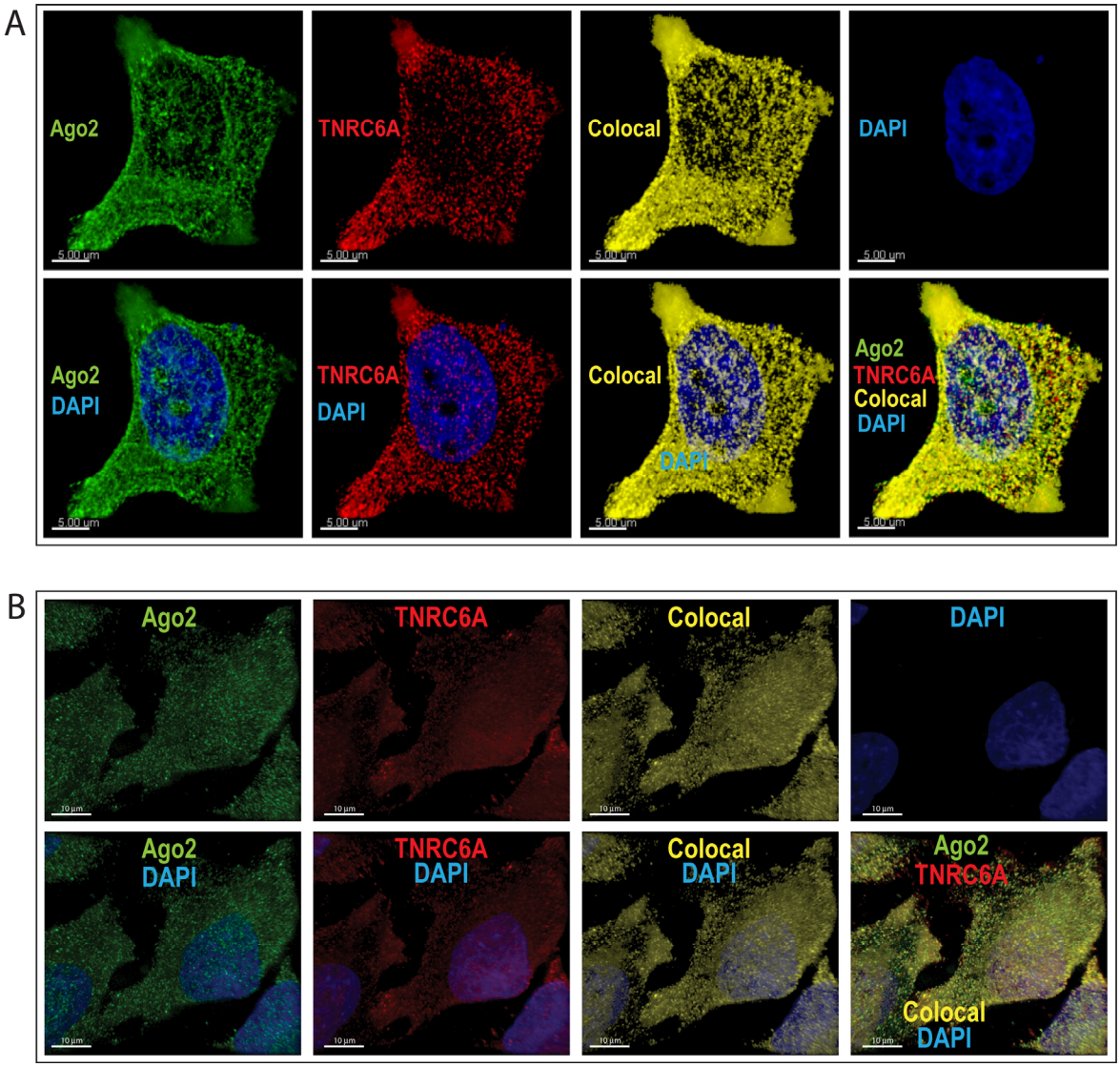

Figure S3, Related to Figure 3: Ago2 and TNRC6A immuno-staining co-localizes in HeLa cell nuclei. Cells were stained with anti-Ago2 from Abcam (**A**) or anti-Ago2 from Wako Chemicals (**B**) and anti-TNRC6A from Bethyl Laboratories (see Methods). (**A**) 4 µm thick and (**B**) 5 µm thick Z-stacks were taken. Co-localization channels were built in Imaris (Bitplane). Scale bars = 10 µm (**A**) and 5 µm (**B**).

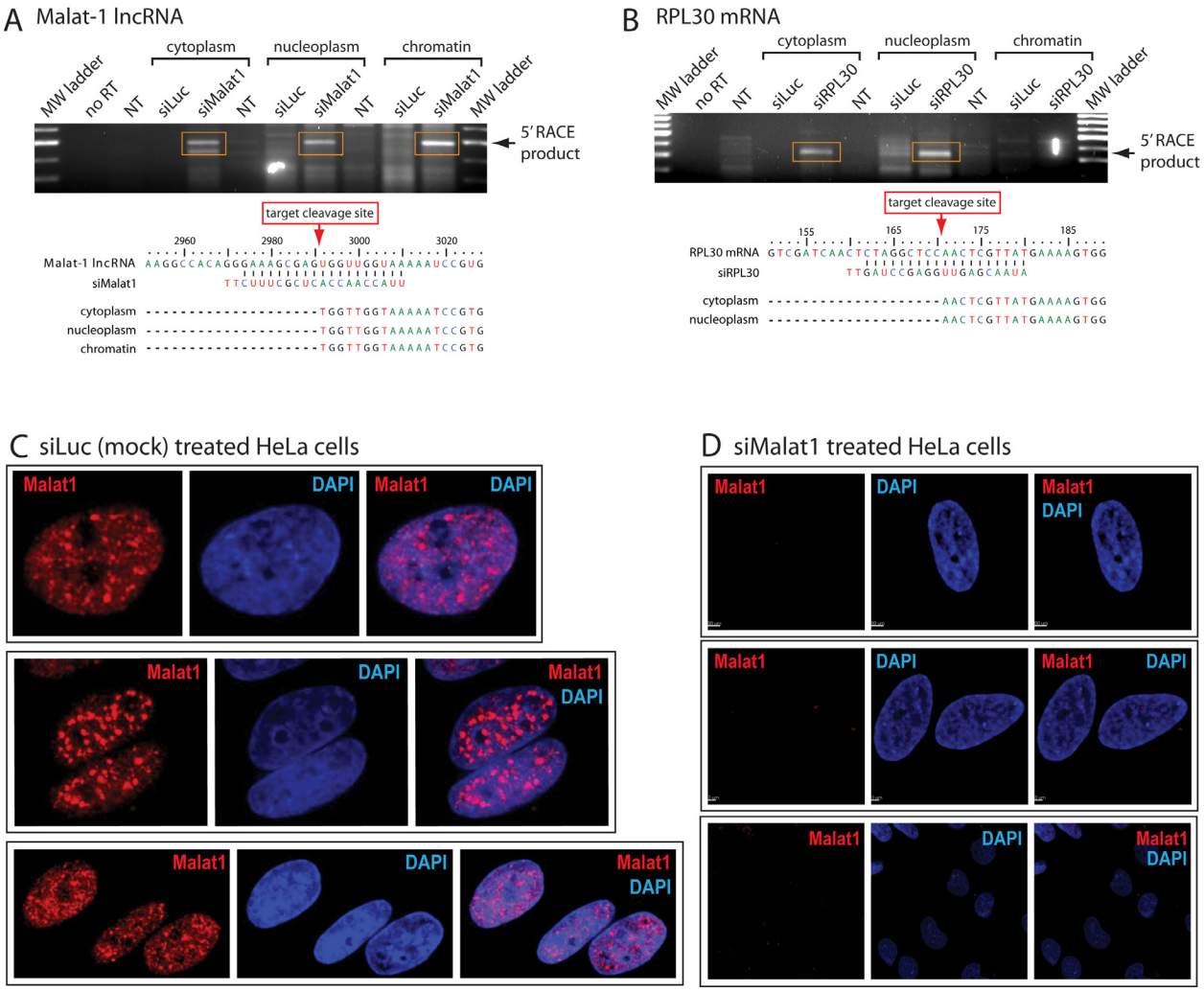

Figure S4, Related to Figure 4: 5'-RACE and Malat-1 FISH demonstrate siRNA-directed cleavage in nuclear fractions. HeLa cells were transfected with siRNA against Malat-1 lncRNA, RPL30 mRNA, with a negative control siRNA (siLuc) or left untreated. RNA from cytoplasmic, nucleoplasmic and chromatin fractions were isolated 72 h post-transfection and subjected to 5'RACE to detect predicted cleavage products for (**A**) Malat-1 or (**B**) RPL30 (see Methods). Gels for separation of RACE products are shown with the cleavage product band highlighted. Cleavage product bands were excised and sequenced to unambiguously validate sequence-specific siRNA-directed cleavage at the expected phosphodiester bond of the targeted RNA. 5' ends of sequenced RACE products are shown below each gel for each cell fraction. RACE was performed at least twice and cloning and sequencing performed several times per band for each experiment. HeLa cells were treated with (**C**) a mock siRNA (siLuc) or (**D**) siRNA against Malat-1 (siMalat1) then processed for FISH analysis (see Methods) 48 h later. Z-stacks 6 µm thick were taken.

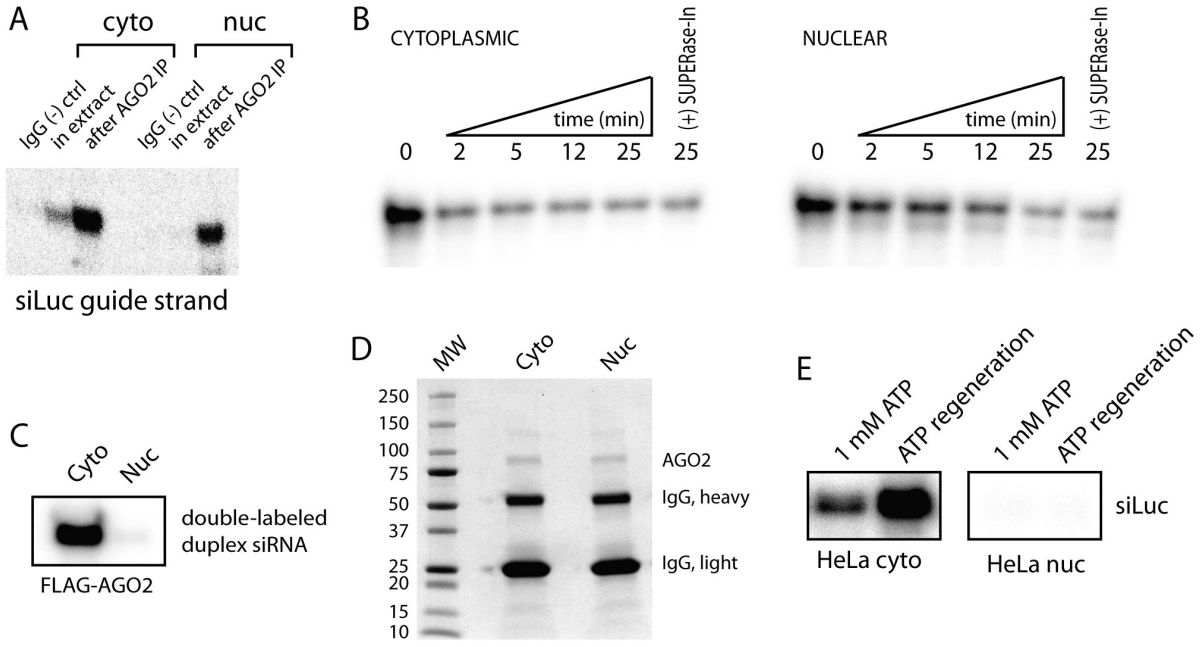

Figure S5, Related to Figure 6: Controls for Ago2 loading deficiency in the human cell nucleus. (**A**) Incubation of single-stranded siLuc guide RNA with T47D cytoplasmic and nuclear extracts followed by Ago2 immunoprecipitation, or with Ago2 after immunoprecipitation. Single-stranded guide RNA does not efficiently bind Ago2 in extracts presumably due to rapid degradation. If Ago2 is first immunoprecipitated to wash away contaminating nucleases, single-stranded guide RNA readily binds and co-immunoprecipitates. (**B**) Degradation kinetics of duplex siLuc in HeLa cytoplasmic or nuclear extracts. (+) SUPERase-In = addition of 50 unites of SUPERase-In RNase inhibitor. (**C**) Ago2 in vitro loading assay using siLuc siRNA dual-labeled on both guide and passenger strands. (**D**) Immunoprecipitation of Ago2 from HeLa cytoplasmic and nuclear extracts followed by coomassie staining shows equivalent amounts of Ago2 capture from both extracts. (**E**) Ago2 in vitro loading assay using radiolabeled siLuc and the addition of ATP regeneration system (see *Extended Methods*) in cytoplasmic or nuclear extracts.

Table S1, Related to Figures 4 and 6 : Small RNAs, primers, probes and oligonucleotides (5' to 3')

siRNAs/miRNAs		
name	sequence	notes
siLuc_as	rUrGrUrUrCrArCrCrUrCrGrArUrArUrGrUrGrCTT	antisense guide strand
siLuc_ss	rGrCrArCrArUrArUrCrGrArGrGrUrGrArArCrATT	sense passenger strand
siLuc_mm_as	rUrGrUrUrCrArCrCrUrGrCrArUrArUrGrUrGrCTT	antisense guide strand
siLuc_mm_ss	rGrCrArCrArUrArUrGrCrArGrGrUrGrArArCrATT	sense passenger strand
siLuc_mm3,6_ss	rGrCrUrCrArArArUrCrGrArGrGrUrGrArArCrATT	sense passenger strand
siLuc_mm9,10_ss	rGrCrArCrArUrArUrCrGrArGrGrUrGrArArCrATT	sense passenger strand
siLuc_mm13,16_ss	rGrCrArCrArUrArUrCrGrArGrCrUrGrUrArCrATT	sense passenger strand
has-miR-19a_5p	rArGrUrUrUrUrGrCrArUrArGrUrUrGrCrArCrUrArCrA	antisense guide strand
has-miR-19a_3p	rUrGrUrGrCrArArArUrCrUrArUrGrCrArArArArCrUrGrA	sense passenger strand
siMalat_as	rUrUrArCrCrArArCrCrArCrUrCrGrCrUrUrUrCTT	antisense guide strand
siMalat_ss	rGrArArArGrCrGrArGrUrGrGrUrUrGrGrUrArATT	sense passenger strand
siNeat_as	rUrUrUrCrUrArArGrCrArArCrUrUrCrUrCrArCTT	antisense guide strand
siNeat_ss	rGrUrGrArGrArArGrUrUrGrCrUrUrArGrArArATT	sense passenger strand
siRPL30_as	rArUrArArCrGrArGrUrUrGrGrArGrCrCrUrArGTT	antisense guide strand
siRPL30_ss	rCrUrArGrGrCrUrCrCrArArCrUrCrGrUrUrArUTT	sense passenger strand
siPPIA_as	rUrUrArGrGrArUrGrArArGrUrUrCrUrCrArUrCTT	antisense guide strand
siPPIA_ss	rGrArUrGrArGrArArCrUrUrCrArUrCrCrUrArATT	sense passenger strand
qPCR		
name	sequence	notes
Malat1 Prime Time Assay F	ACCATCGTTACCTTGAAACCG	forward primer for Malat-1 IDT prime time assay
Malat1 Prime Time Assay R	GATCTAGCACAGACCCTTCAC	reverse primer for Malat-1 IDT prime time assay
Malat1 Prime Time Assay P	/56-FAM/CTCACCTCG/ZEN/ATGCAGCCAGTAGC/3IABkFQ/	probe for Malat-1 IDT prime time assay
Neat1 Prime Time Assay F	TCTCTTCCTCCACCATTACCA	forward primer for Neat-1 IDT prime time assay
Neat1 Prime Time Assay R	CCTCCCTTTAACTTATCCATTCAC	reverse primer for Neat-1 IDT prime time assay
Neat1 Prime Time Assay P	/56-FAM/AACAATACC/ZEN/GACTCCAACAGCCACT/3IABkFQ/	probe for Neat-1 IDT prime time assay
RPL30 Prime Time Assay F	CACCAGTTTTAGCCAACATAGC	forward primer for RPL30 IDT prime time assay
RPL30 Prime Time Assay R	GATCAGACAAGGCAAAGCGA	reverse primer for RPL30 IDT prime time assay
RPL30 Prime Time Assay P	/56-FAM/ACAACTGCC/ZEN/CAGCTTTGAGGAAATCT/3IABkFQ/	probe forRPL30 IDT prime time assay
GAPDH Taqman Assay	proprietary	Applied Biosystems (Hs99999905_m1)
PPIA Taqman Assay	proprietary	Applied Biosystems (Hs99999904_m1)
5' RACE		
name	sequence	notes
GeneRacer RNA Adaptor	rCrGrArCrUrGrGrArGrCrArCrGrArGrGrArCrArCrUrGrA rCrArUrGrGrArCrUrGrArArGrGrArGrUrArGrArArA	5' RACE ligation adaptor
GeneRacer™ 5′ Primer	CGACTGGAGCACGAGGACACTGA	universal forward primer for 5' RACE PCR
GeneRacer™ 5′ Nested Primer	GGACACTGACATGGACTGAAGGAGTA	nested forward primer for 5' RACE PCR
MALAT15RACE1	CCCCCGCCTCAGTTACACATCCA	Malat-1-specific reverse primer for 5' RACE PCR
MALAT15RACE2	CCCCCGCCTCAGTTACACATCCAAA	Malat-1-specific reverse primer for 5' RACE PCR
RPL305RACE	CCGCATGCTGTGCCCAGTTCAAT	RPL30-specific reverse primer for 5' RACE PCR
RPL30-329-76	TCACCAGTCTGTTCTGGCATGCTTC	RPL30-specific reverse primer for 5' RACE nested PCR
RPL30nested-281-78	CAGAGTCACCTGGATCAATGATAGCC	RPL30-specific reverse primer for 5' RACE nested PCR
RPL30nested-202-78	GCCACTGTAGTGATGGACACCAGTTT	RPL30-specific reverse primer for 5' RACE nested PCR
RPL30nested-314-78	CACCAGTCTGTTCTGGCATGCTTCTA	RPL30-specific reverse primer for 5' RACE nested PCR

rN = RNA base; /56-FAM/ = 5' 6-FAM (Fluorescein); /ZEN/ = internal ZEN quencher; /3IABkFQ/ = 3' Iowa Black FQ quencher

Movie S1, Related to Figure 1: 5 µm section from bottom to top of HeLa cells stained with anti-Ago2 (green) from Wako Chemicals. Nuclei are stained with DAPI (blue).